UNIVERZITA KARLOVA V PRAZE

Přírodovědecká fakulta

Katedra aplikované geoinformatiky a kartografie

USING SAR DATA FOR WET SNOW MONITORING

ZJIŠŤOVÁNÍ MOKRÉHO SNĚHU Z RADAROVÝCH DAT

Diplomová práce

Jiří Matyáš

srpen 2014

Vedoucí diplomové práce: Doc. Ing. Jan Kolář, CSc.

Vysoká škola: Univerzita Karlova v Praze **Fakulta:** Přírodovědecká

Katedra: Aplikované geoinformatiky a kartografie **Školní rok:** 2013/2014

Zadání diplomové práce

pro Jiřího Matyáše

obor Kartografie a geoinformatika

Název tématu: Zjišťování mokrého sněhu z radarových dat

Zásady pro vypracování

Cílem předkládané diplomové práce je prostudovat algoritmy používané pro zjišťování vlhkého sněhu z radarových snímků, a z těchto algoritmů jeden vybrat a otestovat. Pro realizaci tohoto úkolu bude třeba také vybrat vhodné území a snímky, na nichž bude vybraný algoritmus testován. Hlavní částí práce bude navrhnout úpravu nebo rozšíření vybrané metody tak, aby poskytovala lepší výsledky. Výsledky

získané upravenou metodou na testovacím území budou porovnány s pozemními daty. Práce bude zpracována v anglickém jazyce.

Rozsah průvodní zprávy: cca 30 stran

Vedoucí diplomové práce: Doc. Ing. Jan Kolář, CSc.

Konzultant diplomové práce:

Datum zadání diplomové práce: 9.6.2014

Termín odevzdání diplomové práce: srpen 2014

Platnost tohoto zadání je po dobu jednoho akademického roku.

……	…….
Doc. Ing. Jan Kolář, CSc.	RNDr. Přemysl Štych, Ph.D.
Vedoucí diplomové práce	Vedoucí katedry

V Praze dne: 9.6.2014

Prohlašuji, že jsem tuto diplomovou práci vypracoval samostatně a že jsem všechny použité prameny řádně citoval.

Jsem si vědom toho, že případné použití výsledků, získaných v této práci, mimo Univerzitu Karlovu v Praze je možné pouze po písemném souhlasu této univerzity.

Svoluji k zapůjčení této práce pro studijní účely a souhlasím s tím, aby byla řádně vedena v evidenci vypůjčovatelů.

V Pardubicích dne 10.8.2014 ……

Jiří Matyáš

Poděkování

Na tomto místě bych rád poděkoval vedoucímu práce, Doc. Ing. Janu Kolářovi, CSc. za čas strávený při konzultacích, trpělivost a cenné rady. Stejně tak bych rád poděkoval Mgr. Veronice Kopačkové, Ph.D., za konzultaci v řešení některých problémů. Dále bych chtěl poděkovat zaměstnancům Norského ředitelství pro vodní toky a energii, zejména Tuomo Salorantovi, za konzultace ohledně použití jejich dat. Poděkování patří také mým rodičům za podporu a trpělivost v průběhu psaní této práce i celého studia.

Using SAR data for wet snow monitoring

Abstract

This paper focuses on an existing method of snow information retrieval by means of satellite SAR data. The method was first presented by Malnes and Guneriussen (2002), and has been proven to be capable of sub-pixel classification of wet snow. It is also able to classify dry snow pixels. The classification is based on change detection, so a snow-free reference image is required. Some flaws in this algorithm have been discovered during the work on this paper and are discussed, as well as a possible solution is suggested. I have also proposed a modification of the algorithm which could improve the classification results and tested the modified algorithm.

Keywords: SAR, snow cover, remote sensing, wet snow

Zjišťování mokrého sněhu z radarových dat

Abstrakt

Tato práce se zaměřuje na existující metodu pro získávání informací o sněhové pokrývce z družicových radarových dat. Zkoumaná metoda byla navržena Malnesem a Guneriussenem (2002) a je schopná provést subpixelovou klasifikaci mokrého sněhu, a také klasifikovat pixely se suchým sněhem. Klasifikace je založená na detekci změn, takže je potřeba referenční snímek bez sněhové pokrývky. V průběhu zpracování byly v algoritmu objeveny některé nedostatky, které jsou v práci diskutovány, a zároveň je navrženo možné řešení. Navrhnul jsem také modifikaci tohoto algoritmu, která by mohla přispět ke zlepšení jeho přesnosti. Modifikovaný algoritmus jsem pak otestoval.

Klíčová slova: SAR, sněhová pokrývka, dálkový průzkum Země, mokrý sníh

CONTENTS

ABBREVIATION LISTING

DEM	Digital Elevation Model
EEA	European Environment Agency
ESA	European Space Agency
CORINE	Coordination of Information on the Environment
IR	Infrared
NEST	NEXT ESA SAR Toolbox
NIR	Near Infrared
NDSI	Normalized Difference Snow Index
NVE	Norges vassdrags- og energidirektorat (Norwegian Water Resources and Energy Directorate)
PRI	Precision Image
SAR	Synthetic Aperture Radar
SCA	Snow Covered Area

FIGURE LISTING

TABLE LISTING

CHAPTER 1

Introduction

1.1 Remote sensing of snow

Land-based methods for measurement of snow properties are precise, but have several disadvantages. Automatic measurement devices are expensive, manual measurements are time-consuming and they are not exactly cheap either. Besides, all of the land-based methods only provide information from a single point, and to get areal data, these point measurements must be interpolated; and interpolation techniques are burdened with errors. Remote sensing, on the other hand, enables collection of data over large areas fast, relatively cheap and repeatedly. However, interpreting the information collected by remote sensing techniques is tricky and requires an intensive research.

Snow data achieved by remote sensing techniques can be useful in hydrological modelling, but also in many other fields. For example the influence of snow covered area and snow properties on animal migration, the animals' condition in spring or condition of vegetation after snow melt can be studied.

However, the most important use of snow observing is snow melt and runoff modelling. Information about snow is a valuable variable in most runoff models. Outputs from such models may help predict increased flood risk, furthermore, spring floods from melting snow are especially difficult to predict. For example, in 1995 the Østland region in southern Norway was struck by one of the strongest floods ever recorded in this part of the country. It was also thanks to remote sensing data that the unusually long-lasting snow cover was discovered, which helped predict the flood and decrease the damage it caused (Moen and Landmark, 2008).

This kind of information is also very important in the hydropower industry. In Norway 98 % of all power comes from hydroelectricity plants (Storvold et al., 2006), while around half of the annual precipitation in Norway comes in the form of snow (Rognes et al., 2005). A majority of Norwegian hydro plants lies in high altitudes and their catchments often cover vast mountainous areas, where regular land-based measurements would be complicated and costly. Knowledge of the amount of water stored in the form of snow, together with the speed of snow melt, is essential to efficiently manage the water level in the reservoir to prevent overflowing or shortage of water. The amount of water stored as snow can also significantly influence the prices of electricity throughout the year (Rognes et al., 2005). For the reasons given in this chapter, most power companies are constantly developing and improving their own runoff models to gain access to the most precise predictions possible. For remote sensing data to be useful in such models, they should not differ from reality by more than 10 % (Storvold et al., 2006). This is why remote sensing of snow is a very active research field in Norway and other Nordic countries. Of course, snow remote sensing is also being actively researched in other regions with significant contribution of snowmelt to annual runoff, like Alpine countries, Himalayan region or Canada.

1.2 Remote sensing of snow: current research status

The Norwegian Water Resources and Energy Directorate (Norges vassdrags- og energidirektorat, NVE) currently uses NOAA (National Oceanic and Atmospheric Administration) AVHRR (Advanced Very High Resolution Radiometer) images operationally to retrieve snow covered area (SCA). This system has been in operational use since the mid-1990s, while the first attempts to retrieve snow information by means of remote sensing began in 1978 (NVE, 2009). This system, however, cannot retrieve information through cloud cover. Such a limitation poses a big problem, because cloud cover is a common phenomenon in Norway, especially during winter. And like this system, all sensors operating in visible or IR part of the electromagnetic spectre are good in retrieving SCA, with some limitations even distinguishing wet and dry snow, but their operational use is strongly limited by the requirement of daylight or cloud-free conditions.

Some operational algorithms for SCA monitoring with radar instruments have also been developed (e.g. Nagler & Rott, 2000). However, most of the algorithms

are good at detecting wet snow, but struggle with detecting dry snow, mostly due to unavailability of a sensor suitable for this purpose. Several workarounds have been developed, but these are still far from perfect. Dry snow was successfully detected with polarimetric data (Martini et al., 2007), but this process requires training data for classification, which reduces the applicability of such algorithm. While trying to get the most out of current instruments, most researchers are also hoping for a future radar instrument that would be better suited for snow monitoring. Current techniques of SCA retrieval from remote sensing data will be discussed in more detail further.

1.3 Thesis objectives

In this paper, existing methods for deriving snow covered area (SCA) from remote sensing data will be described. I will focus mainly on the use of radar instruments, which have repeatedly been used in methods that had promising results, not only for SCA monitoring, but also for monitoring other snow properties, mainly snow water equivalent. Unlike the instruments that operate in the visible or infrared (IR) part of the electromagnetic spectre, radar devices have a big advantage in being able to operate nearly in all meteorological conditions and the ability to gather information at night or through cloud cover. In Norway cloud cover is very common during winter, so radar instruments can provide information much more frequently than instruments operating in other parts of the electromagnetic spectre, which would be often obstructed by clouds. Another advantage of radar systems is that radar waves can penetrate relatively deep under the surface of snow. Thus information from below the snow surface can be gathered, which can help understand the snowpack's properties better.

I will then choose one of the presented methods, modify it, and apply it on a remote sensing data set to gather information about the extent of wet and dry snow. This method's properties, advantages and disadvantages, possibilities of operational use and possible potential for improvement will be discussed. Details about the test data and area of interest will be given further in this paper.

CHAPTER 2

Microwave and radar sensors

Microwave sensors detect radiation of wavelength from about one millimeter up to nearly one meter. The main advantage of using microwave sensors for remote sensing is the ability to penetrate cloud cover, rain or fog and their independence of light conditions, which means they can operate during day as well as at night. However, the radiation intensity of most natural objects on these wavelengths is very low, so data gathered by passive microwave sensors suffer from poor spatial resolution. The reason for this is that for the radiation to be detectable, it must be gathered from a relatively large area.

Radar devices possess the advantages of microwave sensors. In addition, they are equipped with their own source of radiation, so they are not dependent on the intensity of passive radiation of surfaces and therefore can gain a much better spatial resolution. The sensor then records the so-called echo – the strength and form of the signal reflected back to the radar. The echo (also called backscattered signal) contains information about some physical properties of the surface it was reflected from, and its value also depends on signal wavelength and polarization. Strength of the backscattered signal (also known as radar cross section - RCS) is usually measured in square meters, or, generally, units of area. RCS is commonly marked as σ. A simplified way to calculate RCS is given in equation 1, where R is the distance between the radar and the object, E_r is the reflected energy received by the sensor and E_i is the signal's energy when it reaches the object (Mahafza, 2000).

When processing remote sensing radar data, RCS is commonly converted to normalized RCS (σ^o). Normalized RCS is given by equation 2 (NASA JPL, 1994), where A is the image pixel area. Units of σ^o are decibels (dB).

$$\mathbf{1}: \sigma = 4\pi R^2 * \frac{E_r}{E_i} \ [m^2]$$

$$\mathbf{2}: \sigma^0 = 10 * log_{10} * \frac{RCS}{A} [dB]$$

Backscattering coefficient is a simpler way to describe RCS. Backscattering coefficient ρ at wavelength λ is defined as the ratio of backscattered radiation intensity M_r and the intensity of radiation emitted to the surface M_i. The simple formula for computing backscattering coefficient is given in formula 3. Backscattering coefficient represents a surface's ability to reflect radar signal back to its source, by showing how big part of the radiation is reflected back. It is rarely used to describe backscattering intensity in SAR images, even though the term "backscattering coefficient" is commonly used to refer to RCS or normalized RCS. Because of this, it is important to pay attention to the units used to describe backscattering, to be sure what is the author actually referring to.

$$\mathbf{3}: \rho(\lambda) = \frac{M_r(\lambda)}{M_i(\lambda)} * 100\ [\%]$$

2.1 Imaging radar principle

The principle of imaging radar is depicted on figure 1. Radar transmits the signal a little sideways, instead of directly beneath itself. It is important for the radar instrument to be able to determine, where did the backscattered signal come from. Otherwise, backscattered signal from places that lie in the same distance but opposite direction from the nadir would reach the sensor at the same moment and the sensor would not be able to determine which side of the nadir, did the respective backscatters come from. The side-looking principle also allows achieving better ground range resolution. The angle between the radar antenna and the nadir is called look angle, or off-nadir angle and commonly lies between 20 and 50 degrees. The angle at which the signal reaches the ground is slightly higher due to Earth's curvature. The ERS satellite's look angle is 21 degrees and the signal reaches the ground at an angle of 23 degrees (Ferretti et al., 2007).

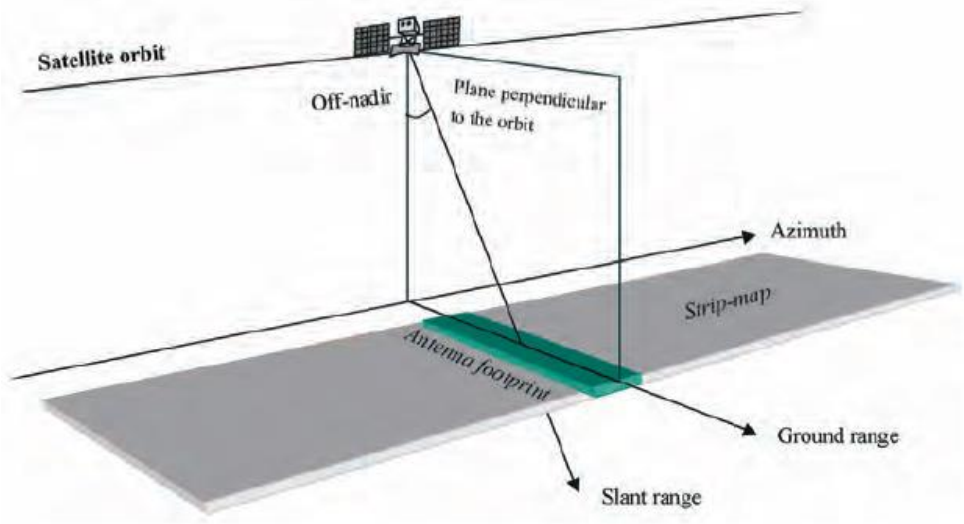

Figure 1:The principle of imaging radar (Ferretti et al., 2007).

Azimuth resolution can be calculated by equation 4 where R_a is azimuth resolution, h is the satellite's height above the terrain, λ is wavelength, L antenna length and θ is the angle at which the signal reaches the ground, or incidence angle (Elachi, 1998 in Finsland, 2007).

$$\mathbf{4}: R_a = \frac{h * \lambda}{L * cos\theta}$$

In case of instruments on the Earth's orbit, their height above terrain is very high. From equation 4 we can see that this leads to either poor azimuth resolution or the need to use a very long antenna or short wavelengths. Shorter wavelengths are, however, more significantly influenced by the Earth's atmosphere and constructing a very long antenna brings some engineering issues. This is why synthetic aperture radars, or SARs, are used.

2.2 Synthetic aperture radar

Synthetic aperture radar (SAR) is a radar system that takes advantage of the Doppler-effect to simulate a longer antenna and improve azimuth resolution. The satellite moves relatively to the terrain, which leads to a change of the backscattered signal's frequency dependent on the speed and direction of the movement related to the scatterer (pixel). The radar signal backscattered from a pixel is being recorded for a certain period of time that depends on the width of the radar beam. During this time period the backscattered signal is being recorded and is further processed as if

it was recorded by an antenna with length equal to the distance the satellite has travelled while recording the signal.

Figure 2 shows how the Doppler-effect relates to SAR. Backscattering from areas b and c will have lower and higher frequency than transmitted respectively, while in case of backscattering from area a there will be no change in frequency. If we imagine the instrument moving forward, signal backscattered from area *a* would have a lower frequency and backscattering frequency from area *c* would not be changed.

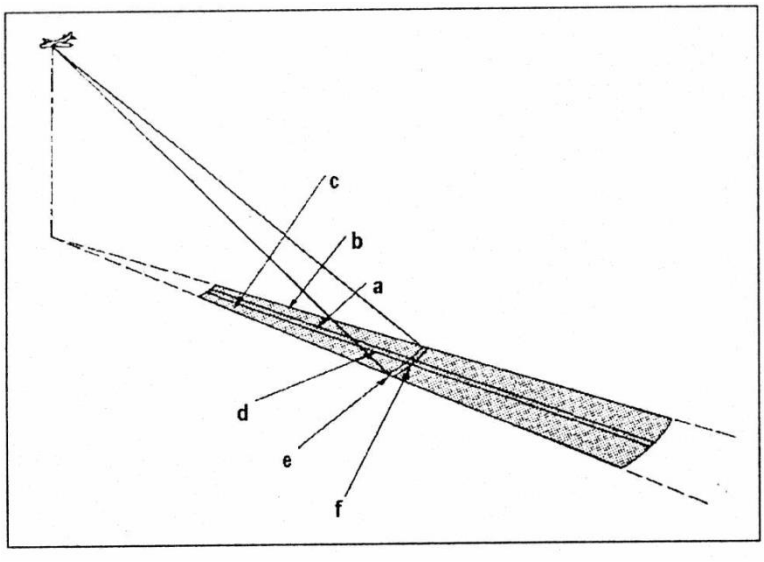

Figure 2: Relation of SAR and the Doppler-effect. a – zero frequency shift, b, c – lower and higher frequency respectively, d – azimuth resolution, e – ground range resolution, f – Resulting pixel. Source: Dobrovolný (1998).

2.3 SAR images geometry and topographic effects

As shown in figure 1, the distance between the radar and an imaged object can be represented in two different ways. Either as slant range, which is the shortest distance between the two objects, or as ground range, which is the distance between nadir and the imaged object. An object's (pixel's) location on a radar image is determined by the time of receiving backscattered signal. This means that a radar is determining the pixels' position by slant range. However, slant range distorts ground range scale – the scale increases with increasing slant range. Slant range can be converted to ground range relatively easily, using the Pythagorean theorem, but such procedure assumes flat terrain (Dobrovolný, 1998). Moreover, a hilly terrain causes several distortions, which are more difficult to correct (or cannot be corrected

at all) and require a digital elevation model (DEM) to be identified. A short description of these distortions follows.

2.3.1 Foreshortening

Foreshortening occurs, when the terrain is sloped against the instrument. It causes slopes on the image to appear shorter than they actually are. In figure 3, the distance of AC is equal to that of AD, but the slant range recorded by SAR shows A'D' significantly shorter than A'C'. The reason is, that backscattered signal from point D reaches the sensor sooner than signal backscattered from C, because D is much closer to the sensor than C. To correct foreshortening we need to know the elevation difference *ΔH*, and incidence angle θ. The shift in the point's position is than calculated by using equation 5 (Finsland, 2007). The equation is explained in figure 3.

$$\mathbf{5}: \Delta g = \frac{\Delta H}{tg\theta}$$

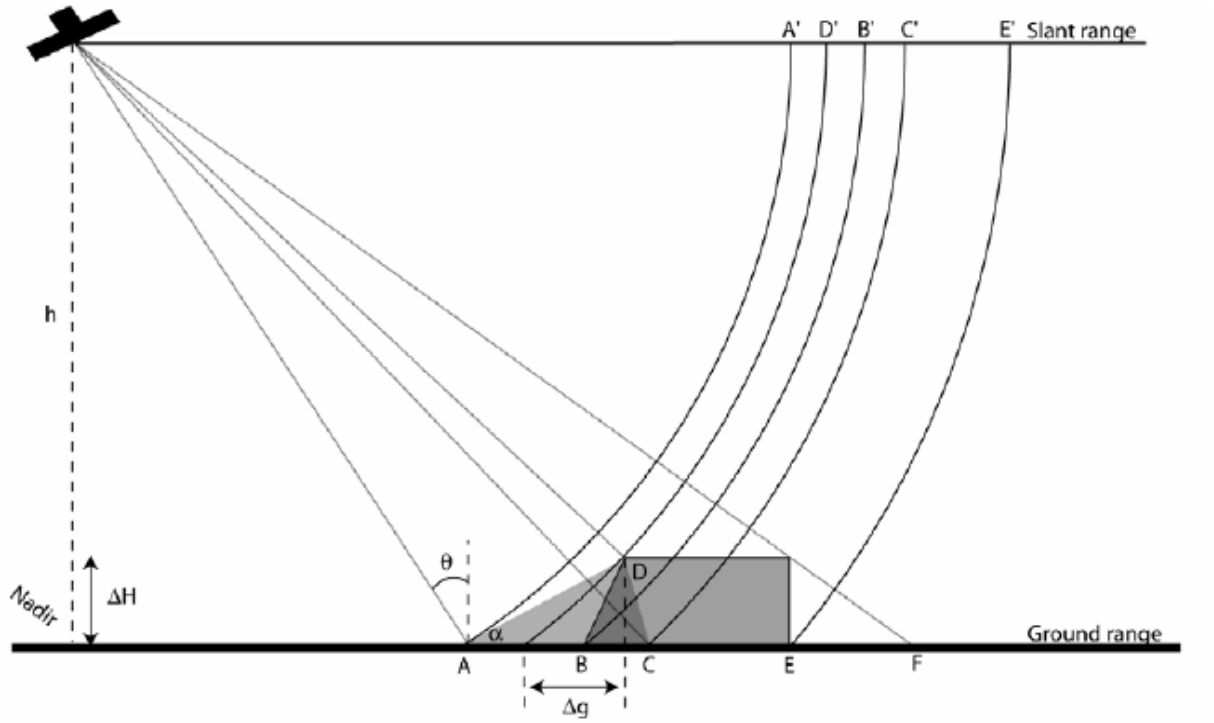

Figure 3: Distortions caused by terrain. Source: Finsland (2007)

2.3.2 Layover

Layover occurs when a hill's slope (α) is bigger than the radar's look angle and at the same time the slope is turned towards the sensor. In case of layover, a mountain top appears before the mountain's foot in the image. This is also shown on figure 3

– D’ appears before B’, even though B is closer to nadir than D. Backscattering from the slope will be melted together and no useful information will be gained from these parts, because echoes from various areas of the slope will arrive in the same time, which makes it seem like they all arrived from the same distance. Echoes from the lower parts of the slope are then laid over echoes from upper parts of the slope, because to the radar it seems like they arrived from the same point. This distortion causes the echo from various, usually not neighbouring, areas on the slope to be combined into one pixel, which makes it impossible to retrieve any kind of reasonable information.

A special case of layover is, if a hill’s slope is equal to the look angle. In this case, backscattering from the entire slope would be recorded at the same moment and the entire slope would be shown as a single pixel with very high backscattering intensity. Also in this case no useful information can be retrieved from the data. For this reason, areas affected by layover are usually masked out during the pre-processing of SAR images.

2.3.3 Shadow

Slopes steeper than the radar’s look angle that are turned away from the radar, cause radar shadow to appear. SAR does not receive any information from areas influenced by shadow, because the radar signal cannot reach these areas at all. In figure 3, shadow occurs between E and F (Finsland, 2007). Also areas affected by shadow are usually masked out from SAR images during the pre-processing phase.

2.4 Radar signal properties & speckle

Parameters of a backscattered radar signal can be divided into two categories – inner parameters, or parameters that are influenced by the radar itself and outer parameters, or parameters influenced by the scatterer. Typical inner parameters are wavelength, signal polarization or look angle. Outer parameters are surface roughness (related to local incidence angle), wetness, topography or the surface’s dielectric properties (Dobrovolný, 1998). The effects of topography have been described in the previous chapter.

2.4.1 Inner properties

Table 1 shows the wavelengths and names for the most common radar bands. Wavelength is an important factor that determines the signal’s ability to penetrate

atmosphere, soil or snow cover. Shorter wavelengths below 3 cm are more influenced by the atmosphere and also have smaller capabilities in penetrating soil and snowpack (Dobrovolný, 1998). Currently, satellite systems operating in bands C (ERS), X (TerraSAR-X) and L (JERS) are active.

Band	Wavelength [cm]	Frequency [MHz]
Ka	0,75 – 1,1	40 000 – 26 500
K	1,1 – 1,67	26 500 – 18 000
Ku	1,67 – 2,4	18 000 – 12 500
X	2,4 – 3,75	12 500 – 8 000
C	3,75 – 7,5	8 000 – 4 000
S	7,5 – 15	4 000 – 2 000
L	15 – 30	2 000 – 1000
P	30 - 100	1 000 - 300

Table 1: Radar bands, according to Dobrovolný (1998).

Radar signal can be polarized. If a signal is not polarized, the wave oscillates in all directions, otherwise only in one plane perpendicular to the signal's direction. Transmitted signal can be polarized either in vertical (V) or horizontal (H) plane. Also the received signal can be filtered by polarization+, which means that a radar signal can be transmitted and received in total four different regimes. Either identical (HH and VV) or unlike (HV and VH) polarization can be used. Signal polarization can be used to gather information about so-called depolarizing surfaces. While comparing

two images with different polarization such a surface would appear different in each image (Dobrovolný, 1998).

Incidence angle has a significant influence on topographic distortions. Large incidence angles cause topographic distortions more often, because a less steep slope is needed for a topographic effect to occur with large incidence angle. Larger incidence angles also make it harder for the signal to penetrate vegetation. At the same time, by increasing incidence angle stronger backscattering from rough surfaces can be achieved (Dobrovolný, 1998).

2.4.2 Outer properties

Radar signal received from a single pixel usually comes from more than one scatterer. In some cases however, a scatterer may cause such an intensive backscatter, that it makes backscattering from all other scatterers in the pixel insignificant and this backscatter will be recorded in the image. A typical example is the corner of a building, which may cause backscatter of nearly all transmitted signal back to the radar (figure 5c). Figure 4 shows a trihedral corner reflector. Despite its relatively small surface, such a reflector will be very well visible on the radar image, because it will return almost all the transmitted signal back to the radar. Unlike a corner of a building, where the reflector is only dihedral, it is less sensitive to the direction from which the signal comes (Finsland, 2007). Trihedral corner reflectors have been used for image calibration and geocoding by, among others, Malnes et al. (2004).

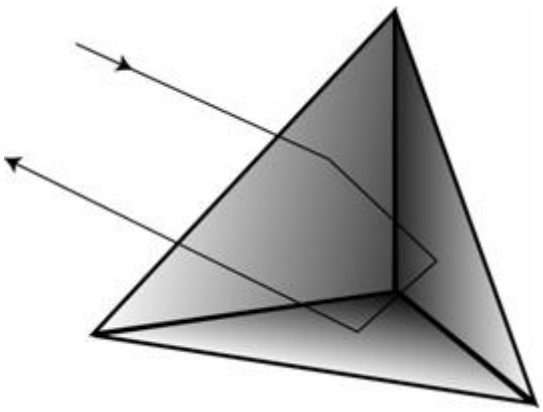

Figure 4: A trihedral corner reflector. Source: Finsland (2007)

Backscattering intensity is a very complex topic and depends on wavelength, polarization, local incidence angle and dielectric and geometric properties of the surface. Different kinds of backscattering depending on surface roughness are

shown in figure 5 – diffusive backscatter, mirror reflection and corner reflection are each shown in 5a, 5b and 5c respectively. Whether or not a diffusive backscatter will occur depends on the surface roughness. Surface roughness is defined relative to wavelength and local incidence angle (Dobrovolný, 1998). According to Kolář et al. (1997), surface roughness is determined by the Rayleigh criterion (formula 6). In formula 6, *rms* is the square root of the unevenness height squared, *λ* is wavelength and θ is local incidence angle.

$$\mathbf{6}: rms > \frac{\lambda}{8 * cos\theta}$$

Formula 6 shows, that a surface can be considered either rough or smooth depending not only on its own properties, but also on the wavelength and local incidence angle.

Kolář et al. (1997) consider a surface rough, when formula 6 is true. Otherwise the surface is considered a mirror reflector. Other authors, for example Dallemand (1993, in Dobrovolný, 1998) relate surface roughness towards average unevenness height.

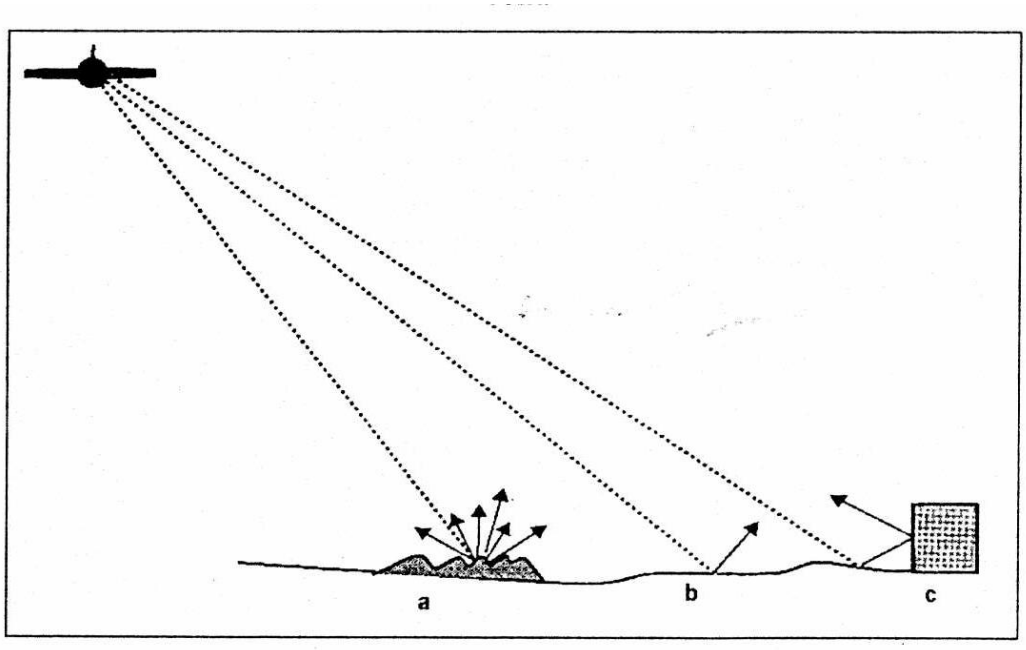

Figure 5: Reflection types depending on surface roughness. Source: Dobrovolný (1998)

With surface roughness as criterion, we may define three different types of scatterers. Diffusive scatterers scatter the signal in all directions, and a part of the

scattered signal is recorded by the sensor. Smooth reflectors reflect most of the signal away from the sensor and no or very little backscatter is recorded. Orientation of the surface to the radar beam also plays an important role. Smooth surfaces that are perpendicular to the radar beam (corner reflectors) will reflect nearly all of the radar signal back to the sensor, which will result in a bright point on the image. Other surfaces with the same roughness but different orientation would, on the other hand, appear as dark points on the image, because most of the signal would be reflected away from the sensor. Corner reflectors are the most common in cities. But even here, orientation of the surface to the sensor plays an important role. Equally rough or smooth surfaces may therefore result in different backscattering intensity depending on the local incidence angle (Dobrovolný, 1998).

Dielectric properties characterize a material's ability to reflect, conduct or absorb electromagnetic energy. To describe them, the dielectric constant is used. Dielectric properties of materials can have a very significant effect on the strength of backscattered signal, especially when liquid water comes into play. Because of the high dielectric constant of water (most commonly, the dielectric constant ranges from 3 to 8, but the dielectric constant of water is 80), the content of liquid water inside a scatterer can significantly influence the intensity of the backscattered signal. Radar backscatter is strongly attenuated by liquid water, which results in a significant decrease of backscattering intensity from wet objects. Changes in backscattering intensity may therefore be related to change of water content in the object, rather than to changes in its other properties (Dobrovolný, 1998).

2.4.3 Speckle

Upon visual inspection, SAR images seem to be very noisy. This happens because the transmitted and backscattered signal has a well-defined phase (i.e. is coherent). This means, that interference occurs between the radiation returned from adjacent parts of the Earth's surface. This phenomenon is called speckle, and can be visually perceived as noise in SAR images. Speckle can be reduced using a number of different filters, at the expense of losing either spatial resolution or some of the details in the image (Pellikka & Rees, 2010).

CHAPTER 3

Snow characteristics and measurement

3.1 Snow formation

When the atmosphere is saturated with water vapour or when air temperature drops below dew point, water vapour in the atmosphere condenses. If the temperature is lower than 0°C at the same time, deposition occurs instead. This means that water transitions from gaseous state directly to solid state. This process is sometimes also called crystallization. Gaseous water is deposited in solid (frozen) state on small solid objects contained in the atmosphere, for example dust particles. Water molecules are than agglomerated into crystalline formations – snow crystals.

Snow crystals can possess a nearly unlimited range of different shapes and sizes, depending on the amount of gaseous water in the atmosphere or temperature during condensation. At low air temperatures, only single snow crystals are observed, while at temperatures nearing 0°C the snow crystals group together to form snowflakes - the higher the temperature the bigger the snowflakes (Doležal and Pollak, 2004).

3.2 Types of snow

Snow cover can be classified in several different ways. Most commonly it is categorized by its texture, grain size and wetness.

If snow is categorized by its texture, criteria like grain size and shape, snow pack compactness or pore size are taken into account. All of these are dependent on the age of snow and on meteorological conditions. Freshly fallen snow is not compact and is the foundation for powder avalanches (Finsland, 2007). It is also easily transported by wind. This type of snow is called fresh or powdery. When fresh snow gets more compact, e.g. because of wind or its own weight, it becomes crud.

Crud is the foundation for slab avalanches (Finsland, 2007). Snow particles in crud are called decomposing or fragmented particles. Granular snow is snow that has been lying for a long time. It can be further categorized according to grain shape as either snow with rounded grains or solid faceted crystals. Last but not least, firn is the type of snow that has been lying for a very long time (most commonly over a year, but sometimes even the last remnants of spring snow are categorized as firn). Firn has often large, round grains and the original snow crystal has been completely metamorphosed (Doležal and Pollak, 2004).

Category	Grain size [mm]
Very fine grains	<0.2
Fine grains	0.2 – 0.5
Medium grains	0.5 – 1.0
Coarse grains	1.0 – 2.0
Very coarse grains	2.50 – 5.0
Extremely coarse grains	> 5.0

Table 2: Snow grain size classification according to Doležal and Pollak (2004).

Snow classification by grain size according to Doležal and Pollak (2004) is shown in table 2 while table 3 shows the same authors' idea of classifying snow according to its wetness, or liquid water content. In this paper however, I will be only using two classes of snow wetness – wet snow and dry snow. The reason for this is the fact, that there are currently no known remote sensing techniques, which would allow to attempt distinguishing more classes.

Category	Average liquid water content [%]
Dry snow	0
Moist snow	< 3
Wet snow	3 – 8
Very wet snow	8 – 15
Extremely wet snow	> 15

Table 3: Snow wetness classification according to Doležal and Pollak (2004).

3.3 Land-based measurements of snow characteristics

Snow depth, grain size, or snow water equivalent are among the most commonly measured snow properties. Furthermore, analysis of snowpack stratification is often performed in order to evaluate the snowpack's stability and avalanche risk. Snow water equivalent is usually presented in millimetres and describes the depth of water that would result from melting of all snow covering an area of one squared meter. It is likely to be the most valuable variable that can be used in snowmelt and runoff modelling, because it states exactly how much water is stored within the snowpack.

The traditional measurement techniques are rather simple. Depth is simply measured using a long probe. For measuring water equivalent, one first takes a snow sample of known volume. For gathering such a sample, NVE (2008) recommends using a one meter long metal (preferably steel or aluminium) cylinder with a diameter of ten centimetres, and sharp edges on its lower side to cut through snow easily. A hole in the snowpack (all the way to bare ground) shouod be dug to allow easier manipulation with the cylinder. A sample is then taken with the cylinder, near the edge of the hole. If the snow is deeper than the cylinder, samples are continuously taken until one reaches the ground. For each sample we measure its weight and, if the cylinder is not full (in case of the last sample before reaching bare ground), also

its volume is measured. From these measurements one can easily compute the snow's density and using snow depth also snow water equivalent.

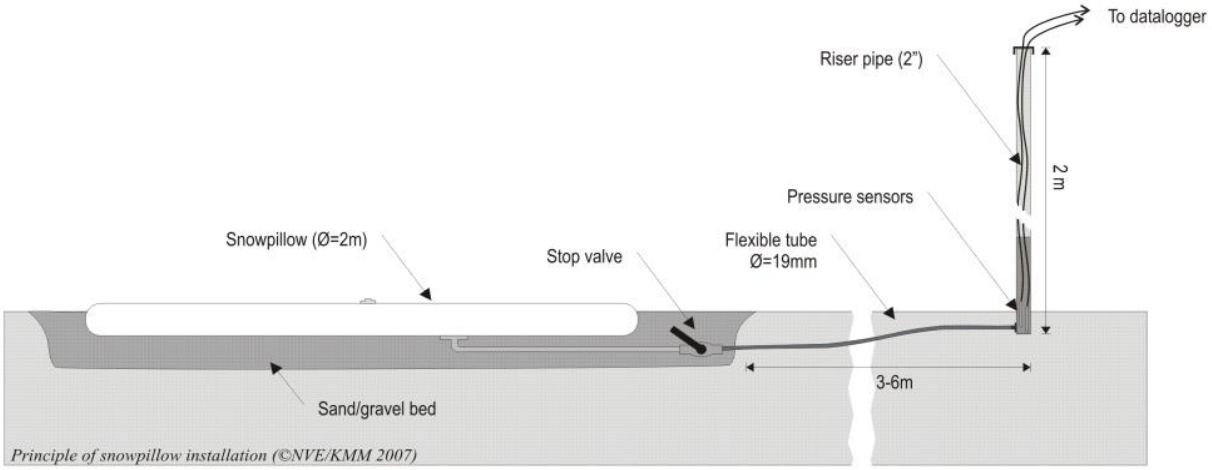

Figure 6: The principle of snow pillows. Source: NVE (c2007)

For automatic measurements of snow water equivalent, so called snow pillows are used. These pillows measure the weight of snow from which snow water equivalent is computed. The way such devices work is shown on figure 6. Unfortunately, these devices are not cheap, so for example in the entire Norway, automatic snow water equivalent measurements are only performed by 25 snow pillows. Norway being a country with a high interest in snow monitoring and a much better financial situation than most other countries, suggests that most other countries will have a much thinner automatic SWE measurement network, if any at all.

3.4 Remote sensing-based retrieval of snow properties

3.4.1 Microwave backscattering from snow-covered terrain

Backscattering from snowpack is a result of the influence of three components. These mechanisms of backscattering for a homogenous layer of snow are depicted in figure 10, A being backscattering from snow-air interface, B volume scattering from the snowpack and C Backscattering from the underlying ground. If the snowpack is not homogenous and consists of more layers, the boundaries between these layers also contribute to backscattering, as well as each layer's volume.

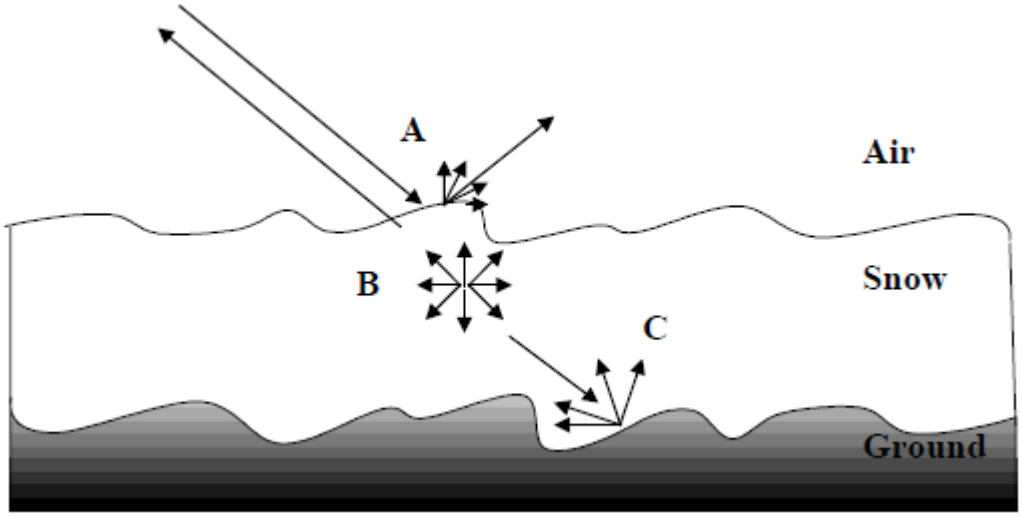

Figure 10: Backscattering mechanism from a homogenous snowpack. Source: Koskinen(2001)

3.4.1.1 The effect of snow wetness on backscattering

In case of dry snow, the dielectric contrast at the air-snow interface is very low and so is the backscatter intensity. This means that the backscattering from air-snow interface in the case of dry snow could be neglected. Also volume scattering has low significance, but increases with increasing depth of the snow pack, as the signal is attenuated and the ground's contribution to total backscattering decreases. Furthermore, the low dielectric contrast causes the importance of snow roughness or grain size to diminish. The backscattering of dry snow also decreases with increasing incidence angle. This is caused by decreasing contribution from the ground, as the incidence angle increases. The influence of incidence angle was computed by Koskinen (2001) using a model, and the result is shown in figure 11. This is important to bear in mind when comparing multiple products with varying incidence angles.

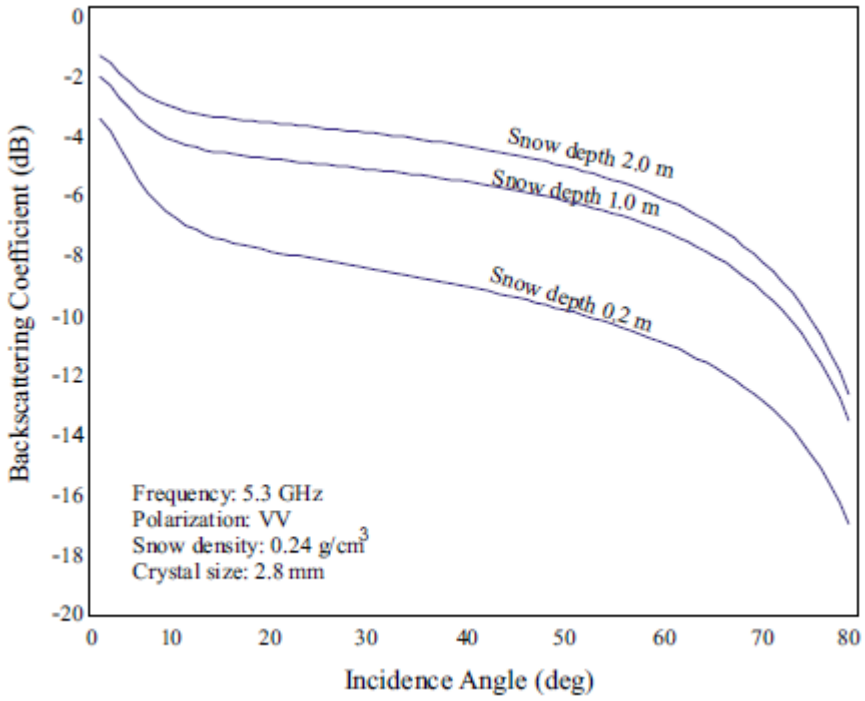

Figure 11: The effect of snow depth on backscattering coefficient as a function of incidence angle. Source: Koskinen (2001).

When the snowpack is wet, the water contained in the snowpack absorbs some of the signal. This is why an increase in snow wetness (also meaning an increase of liquid water content) leads to decreasing contribution of the ground to the total backscattering. The wetter the snowpack, the more radar signal is absorbed and not backscattered. Therefore the total backscattering decreases with increasing snowpack wetness, which is shown in figure 12. The influence of incidence angle on backscattering as a function of snow wetness has also been modelled in figure 12. The simulation has been performed by Koskinen (2001). Increasing incidence angle leads to a decreasing backscattering intensity, but the general functional behaviour remains the same for any incidence angle. This means that the backscatter decreases nearly linearly until around 2% of wetness for any incidence angle. After reaching around 2% wetness the curve stops the rapid decrease and levels out.

Snow wetness also causes an increase of the dielectric contrast at the snow-air interface, which results in a higher contribution of this interface to total backscattering and to increasing significance of surface roughness. In fact, if the snow is wet enough, surface backscattering may even be the most significant component in total backscattering. Therefore, snow surface roughness is very important to be accounted for when modelling backscattering of wet snow.

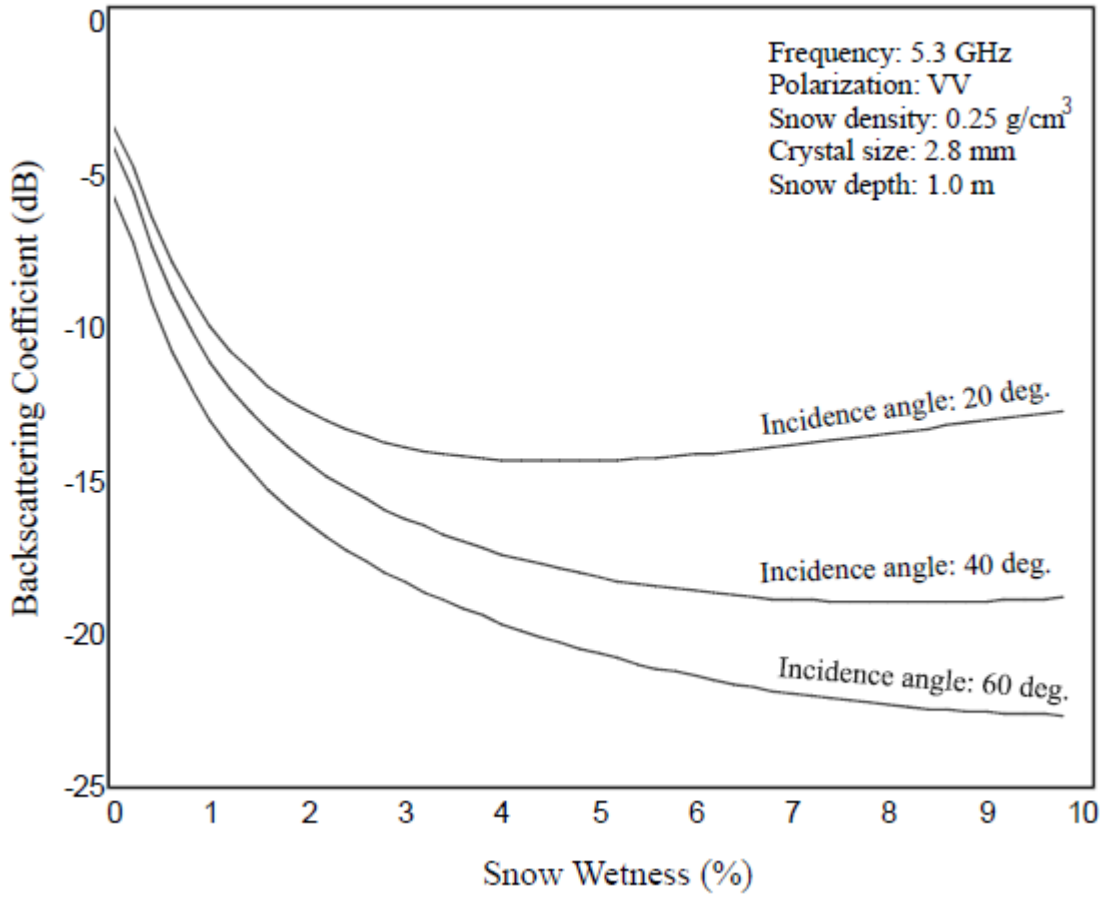

Figure 12: The effect of snow wetness on backscattering coefficient. Modelled by Koskinen(2001).

Figure 13 shows the diurnal behaviour of snow wetness as well as backscattering coefficient on various microwave frequencies. Unlike figures 11 and 12, the data in figure 13 represent actual observations. These observations show that snow wetness may vary significantly throughout the day, depending on changing air temperature or sunshine. Based on the data from figure 13, one should be very careful when interpreting the results of a remote sensing-based snow wetness analysis, because the reference data may have been taken in a different time of the day than the interpreted images. This must therefore be taken into account when evaluating the results of this paper and when working with data from multiple passes.

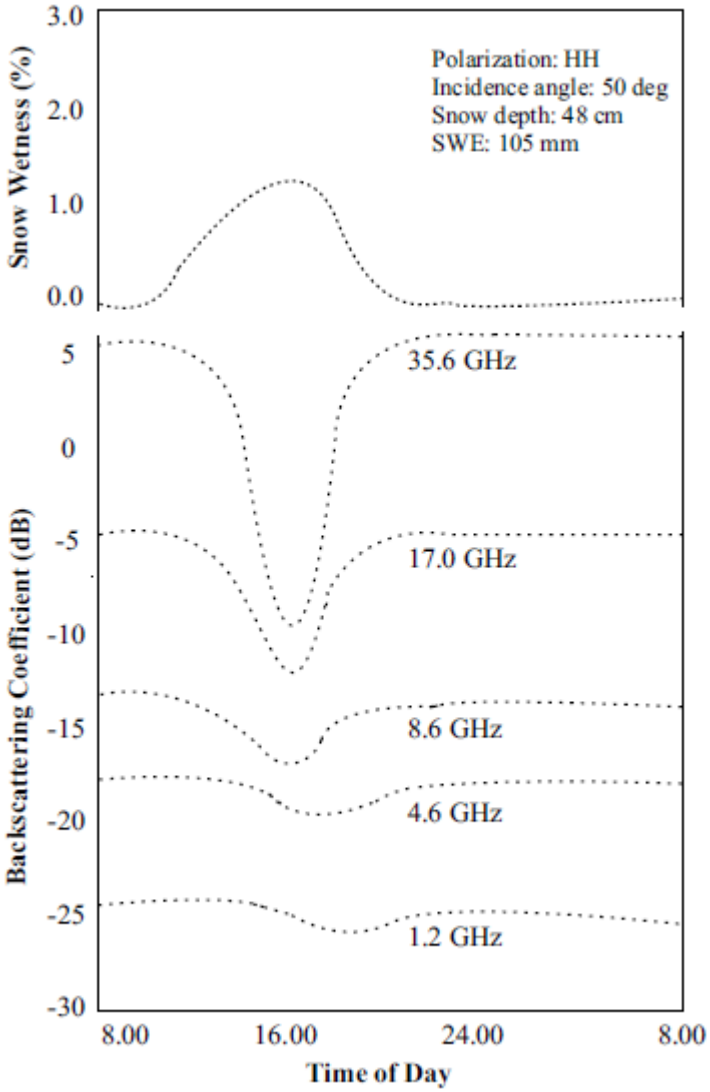

Figure 13: The diurnal pattern of snow wetness and backscattering coefficient. As observed by Koskinen(2001).

From figure 13 we can also see that higher frequencies respond to changes in snow wetness more drastically. This is because high frequencies do not penetrate so deep into the snowpack and the total backscatter is dominated by backscattering from the air-snow interface. High frequencies, like Ku- or K-band, may therefore be useful in monitoring dry snow. A single satellite radar, operating on multiple frequencies and polarizations, could therefore gather information simultaneously from the air-snow interface, the snowpack and the snow-ground interface, because each of these responds to different frequencies. Many authors, like Koskinen (2001), have expressed their hopes for a future multi-channel SAR instrument that would allow better operational snow monitoring. Such an instrument, unfortunately, is

unlikely to be launched in the near future, and that is why it is still attractive to try and find an operationally-useable method for snow monitoring using one of the currently operational radar instruments.

We can thus summarize that:

- Wet snow has significantly lower backscattering coefficient than dry snow.
- Dry snow will probably be difficult to distinguish from bare ground, especially on lower frequencies like C-band.
- Each part of the snowpack responds differently to different wavelengths which makes it nearly impossible to gather information about the entire snowpack.
- Most of the backscattering from a wet snowpack comes from the snowpack's volume scattering and the air-snow interface; the signal does not reach the ground in deep snowpack.
- In the case of dry snow, most backscattering comes from the ground and some from the snowpack's volume scattering.
- Snow backscattering coefficient decreases nearly linearly until 2% of snow wetness. The favourable limit for wet snow could therefore be 2% of volumetric wetness.
- The backscattering coefficient is strongly related to the snow's wetness
- Snow wetness, as well as backscattering coefficient, changes significantly throughout the day.
- The total backscattering coefficient changes with incidence angle, but the functional behaviour remains the same.

3.4.1.2 SAR capabilities in snow-covered area and wet snow monitoring

SAR instruments have however been a bit more successful in retrieving SCA, especially wet-snow cover, and some operational algorithms have already been developed (see for example Nagler and Rott, 2000). However, these algorithms are still far from perfect. The biggest flaw in using SAR for snow monitoring is the fact, that on SAR images retrieved from currently operational instruments it is impossible to distinguish dry snow from snow-free ground (Koskinen, 2001), so alternative methods are used to retrieve dry-snow covered area, such as assuming that all pixels that have not been classified as wet snow and lie above the average (or median) altitude of pixels classified as wet snow are dry snow. Surprisingly enough, such techniques perform quite well.

Some results which suggest that dry snow mapping with C-band SAR might be possible, have also emerged. For example Pivot (2012) has discovered, that in C-band under certain conditions (the first 20 cm of soil penetrated by frost, and incidence angle between 20 and 31°), each 5-10 mm of accumulated water equivalent increases the total backscatter by 1 dB. These results have however not been verified, so it is not advisable to rely on them.

Property	**Visible/NIR**	**IR**	**Microwave**
Snow extent (SCA)	Yes	Yes	Yes
SWE	Fair *(shallow snow only)*	Poor	Fair
All weather capability	No	No	Yes
Spatial Resolution	~10 m	~100 m	*Passive sensors 20 – 150 km* *Active sensors ~30 m*

Table 4: Remote sensing instruments' capabilities in retrieval of some snow

characteristics according to Rango (1986) in Koskinen (2001).

Table 4 summarizes the capabilities of various types of remote sensing instruments in retrieval of snow properties. As mentioned before, microwave and especially SAR instruments are likely to be the best choice for operational snow monitoring, because of their good capabilities in retrieving the information, their independence on weather conditions and a reasonable spatial resolution.

Probably the most significant weakness of SAR data in snow monitoring is the behaviour of SAR signal on various land-use and land-cover types, the most widely discussed and examined being various forest classes. A forest backscatter model is usually used to separate backscatter from ground and forest. A different backscatter model is required for different forest types. Monitoring snow cover in forests is a separate research topic, commonly addressed by, among others, researchers from Finland – for example Koskinen et al. (2010). Most researchers, however, use a land cover map to mask out forests and other land cover types that could potentially cause problems in snow classification (like water), so that they can focus on classifying snow in open areas, which is still an active research topic itself.

3.4.2 Snow water equivalent monitoring with SAR

Measuring snow water equivalent (SWE) with SAR is an active research topic. The delta-k technique, first presented by Engen et al. (2003), has shown promising results. However, this method has several drawbacks that would make its operational use very complicated. Some of these drawbacks are the possibility of measuring only dry snow's SWE, the need for precise calibration and deployment of corner reflectors in the investigated area or the need to average to larger pixel size, which results in poor spatial resolution. Furthermore, current satellite-borne SAR instruments are far from ideal for SWE monitoring and using other bands, like Ku-band, (or even multiple bands used by the same instrument) have been suggested in order to improve the results. However, it seems unlikely that a new SAR instrument with specifications better for SWE monitoring will be launched any time soon (although there is some ongoing research in this area – see further), so finding a better SWE retrieval algorithm for C-band SAR is currently the best way to make progress in this area.

To improve the capability of monitoring SWE and SCA, but also other hydrological variables, the Cold Regions Hydrology High-resolution Observatory (CoReH2O) mission has been proposed (see Rott et al., 2010). The proposed instrument is a dual-frequency (X-band and Ku-band) dual-polarization SAR. However, it is not yet clear when, and if, this mission will be launched, so active research still needs to focus on current SAR instruments.

I have chosen to not investigate SWE retrieval furher, because current SAR instruments do not seem to have the potential to provide the required information with sufficient accuracy, and even though some methods seem to be promising, their implementation is too complicated for a single student to carry them out, because the procedure requires a certain budget and also manpower.

3.4.3 Snow-covered area and wet snow monitoring with SAR

Using SAR for monitoring Snow-covered area is an active research field. As one can easily deduce from chapter 3.4.2, identifying wet snow from SAR data is relatively easy. However, identifying dry snow is a much more difficult task, and several different techniques have been developed, with varying success. In this chapter, I will describe recent techniques for retrieving wet and/or dry snow cover information. The techniques most important for this paper will be discussed more thoroughly in their own subchapters.

3.4.3.1 Thresholding techniques

For wet snow identification, thresholding techniques are the most common and also most straightforward. As I mentioned in chapter 3.5.1, the presence of liquid water in the snowpack significantly reduces backscatter. The backscatter is much less intensive than backscatter from snow-free ground and this behaviour has been exploited by several researchers for mapping wet snow cover. In general, these techniques usually require a snow-free or dry-snow reference image. The difference between backscatter from the reference image and the image of interest is then calculated. If the difference exceeds a certain threshold, the corresponding pixel is classified as wet snow.

Most commonly, the threshold is set around -3 dB, but most researchers usually experiment with the threshold value. Some, like Malnes and Guneriussen

(2002) even used a “soft” threshold (see chapter 4.3.1.3) to enable sub-pixel classification.

Valenti, Small and Meier (2008) used the thresholding technique for monitoring snow cover with multi-temporal ENVISAT ASAR data. The images were classified using a qualitative RGB overlay method. Temporal and spatial variations of backscatter in different scenes than appeared as a primary colour or a combination of them. The resulting comparison of a dry snow reference image with images taken during the melting season indicates differences in snow properties. This way, melting and freezing cycles can be monitored. Valenti, Small and Meier (2008) have found, that the backscatter differences caused by melting snow usually range from -3 dB to -12 dB. Another useful information is, that a robust radiometric correction of terrain-induced local incidence angle variations improves thematic information retrieval.

Slightly different approach was used by Bartsch et al. (2007). A combination of ascending and descending orbit images were used to reduce loss of information due to topographic effects. The most fundamental difference is, that Bartsch et al. (2007) did not convert backscatter to dB, as is the common practice, but used linear backscatter ratio values instead, and calculated the ration between reference image and the image of interest. The ratio images were then classified. The threshold was ratio less than 1 for morning acquisitions at the beginning of snow melt, and all further images were classified using a value of 2. This means that a reduction to at least a half of backscatter was assumed. The final step was to combine the results from ascending and descending orbits by deriving probability classes from the classified images. What Bartsch et al. (2007) called ‘Thawing snow with high probability’ is assumed if significant backscatter decrease was detected in both (morning and evening) images. Medium probability was assumed if melting snow was detected in either morning or evening image, and if no data could be acquired due to layover or shadow effects in the other image. Finally, low probability is assumed if low backscatter decrease was detected in one image, and high backscatter decrease was detected in the other image. The results were compared with SPOT data, taken 4 days after the SAR acquisitions and were found to be promising, but the results were not described in detail.

One of the most recent papers based on a thresholding technique was presented by Thakur et al. (2013). In this study, SAR data from Radarsat 2 and ENVISAT ASAR were used, together with MODIS 8 day global LST product. Pixels with land surface temperature less than -1 °C were classified as dry snow and other pixels were considered for wet snow mapping. The wet snow mapping algorithm classified pixels as wet snow if the difference between backscattering from reference (dry snow) and classified image is less than a certain threshold. In this case, the threshold value varied between -2 dB and -3 dB. Also, only pixels with backscattering values in a certain range ($a < \sigma^0 < b$) were considered for wet snow classification, which was found to increase classification accuracy significantly. The most suitable parameters were found to be -24 dB and -4 dB respectively. The results were promising, and the SAR derived SCA was said to correspond well to MODIS 8-day SCA products, but, like in most similar studies, the possibilities to verify results were very limited.

3.4.3.1.1 The Koskinen method

The Koskinen method estimates the fraction of wet snow covered ground and is based on comparing the test image with two reference images. One of the reference images is fully covered with wet snow and the other one is snow-free.

The need for a reference image fully covered with wet snow suggests that this procedure can be hardly used in regions with complicated topography, because in such areas snow wetness can vary significantly on short distances, which would require a large amount of reference images, as each image would only contain a small area with wet snow cover. Koskinen (2001) has tested his algorithm in a rather flat and homogenous area in northern Finland, which is feasible for this method. But the test area used in this paper (see chapter 4) is far from homogenous, as there are strong climatic differences between valley floors and the plateau and also significant differences in climate between east (more continental climate) and west (climate more significantly influenced by the ocean). These phenomena do not occur so strongly on such short distances in Finland.

Furthermore, Koskinen's method is only used to distinguish wet snow from other snow/ground conditions, whereas in this paper I aim to map both dry and wet snow cover. It is, however, a good starting point.

This method uses a linear relationship between backscattering observed in the snow-free reference image and in the wet-snow-covered reference image to calculate the percentage of area covered by wet snow. However, the results are mostly just two classes: wet snow and no wet snow. Just a few pixels contain an intermediate value.

The results achieved by the classification algorithm have been compared to visual observations, which means, that the results presented in his paper are very rough and “only” prove that there is a relationship between the SAR-derived information and field observations. But even this is a success and a good fundament for future research, as well as it shows that one of the most crucial and complicated parts of any similar research is obtaining a reasonably detailed and precise ground-truth data set. As I have mentioned before, retrieving ground-truth data requires resources (both financial, technical and human) that most researchers will struggle to obtain.

3.4.3.1.2 The Nagler & Rott method

Nagler & Rott (2000) use a simple thresholding algorithm to detect wet snow. They have found that the change in backscattering between the reference image and the wet snow image of -3 dB to be an appropriate threshold for their test area.

Use of images taken from opposite passes has also been suggested in order to reduce the area affected by shadow and layover and thus obtain information from a larger area. Furthermore, it was Nagler & Rott (2000) that have successfully used an image under dry snow conditions as a reference image. It has also been suggested to use a different classification approach for different land cover classes, namely agricultural areas that can be affected by surface roughness change, and mires that can be affected by wetness under snow-free conditions. It is either possible to avoid misclassifications on such areas by using land cover maps, topographic information or by studying the seasonal behaviour of backscattering from these areas.

Basically, the decision making of their algorithm is very simple – if a pixel is affected by layover, radar shadow or inappropriate local incidence angles in both passes, then snow mapping is not possible. If not, then the backscattering change between the test image and the reference image is calculated. If the result is less

than -3 dB, than the pixel is covered by wet snow, otherwise it is covered by either dry snow or bare ground.

Landsat TM images and photographs taken on the day of the radar pass were used by Nagler & Rott (2000) to verify their results. However, the Landsat data cannot provide proper information on snow wetness. On the other hand, on one of their test images all of the remaining snowpack was supposedly wet. Overall, they have achieved 83% agreement between the ERS and Landsat images.

Temporal consistency of SAR-derived snow maps was also investigated by Nagler & Rott (2000). It was based on the assumption, that pixels once classified as snow-free should remain snow-free later in the season, in case no fresh snow falls. A pixel by pixel comparison showed that 3.2 % of pixels classified as snow-free in June were classified as wet snow in July. This inconsistency is said to might have been caused by level of multi-looking and speckle filtering or by inaccurate geocoding and coregistration.

This approach has been used by Pettinato et al. (2009) to develop an operational snow-mapping algorithm. The algorithm in question uses MODIS data when possible (cloud-free conditions) and ENVISAT ASAR data for areas covered with clouds. ENVISAT data are classified using the Nagler & Rott (2000) approach, so they can only be used to identify wet snow. Snow on MODIS data is classified using the Normalized Difference Snow Index (NDSI). The information output of this algorithm is inconsistent, as pixels not affected by cloud cover are classified either as snow-free or snow covered, while the rest is classified as either wet snow or no wet snow.

3.4.3.1.3 The Malnes method

Malnes and Guneriussen (2002) have based their research on the two methods mentioned previously. The result of their work is a sub-pixel classification of wet snow, which, together with a reasonably detailed DEM, can also detect dry snow. For simplicity's sake, I will refer to their algorithm as to the "Malnes' algorithm" from now on.

Malnes' algorithm masks out forest and water, because these two land cover classes give ambiguous results in SAR SCA mapping. Also pixels affected by

shadow or layover are masked out. The remaining pixels are than classified using modified Nagler's & Rott's (2000) algorithm. Resulting classification classes are snow-free ground, pixels containing 0 – 100 % of wet snow and dry snow.

The technique employed to obtain percentage of wet snow cover in a pixel originates from the -3 dB classification threshold found by Nagler & Rott (2000) and the linear sub-pixel classification scheme used by Koskinen (2001). Malnes and Guneriussen (2002) have, however, found, that using a "soft" threshold centered around -3 dB together with the sigmoid function shown in formula 7 (*x* being the backscatter and *a* being a slope parameter for the function – see figure 19) gives more information than the "hard" threshold used by Nagler & Rott (2000). The percentage of wet snow cover on each pixel is derived from the sigmoid function. Figure 14 shows the sigmoid function used for sub-pixel classification.

$$\mathbf{7}: F(x) = 50 - 50 * \tanh[a * (x + 3)] \ \%$$

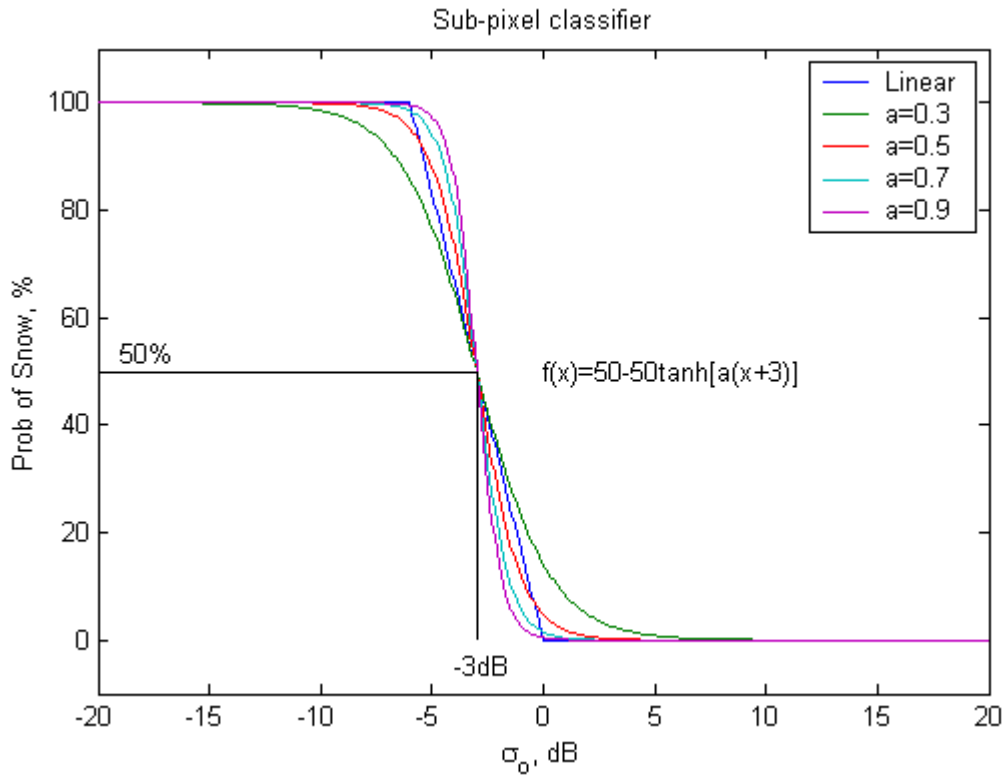

Figure 14: Weight function for sub-pixel classification of wet snow. When the difference is below 0 dB, snow is classified as 0 – 100% wet. Source: Malnes and Guneriussen (2002)

Another improvement of Malnes' algorithm is, that after performing the wet snow classification, it is possible to postulate that all pixels that lie above the median

altitude of wet snow and that are not classified as wet snow, can be classified as dry snow. This is applicable in Norwegian mountains, but does not have to apply in other regions, like the Alps, where mountain tops may be snow-free due to wind (Malnes and Guneriussen, 2002)

Malnes and Guneriussen (2002) have also suggested a special classification scheme for water bodies and suggest that other land uses can be processed in a similar manner. In this paper, I will attempt to process water bodies separately.

Statistical methods have been used by Malnes and Guneriussen (2002) to calculate the error rate achieved by their algorithm, because the authors were not able to find any suitable optical images. The resulting overall error rate was computed to be 16.6 % (see figure 15).

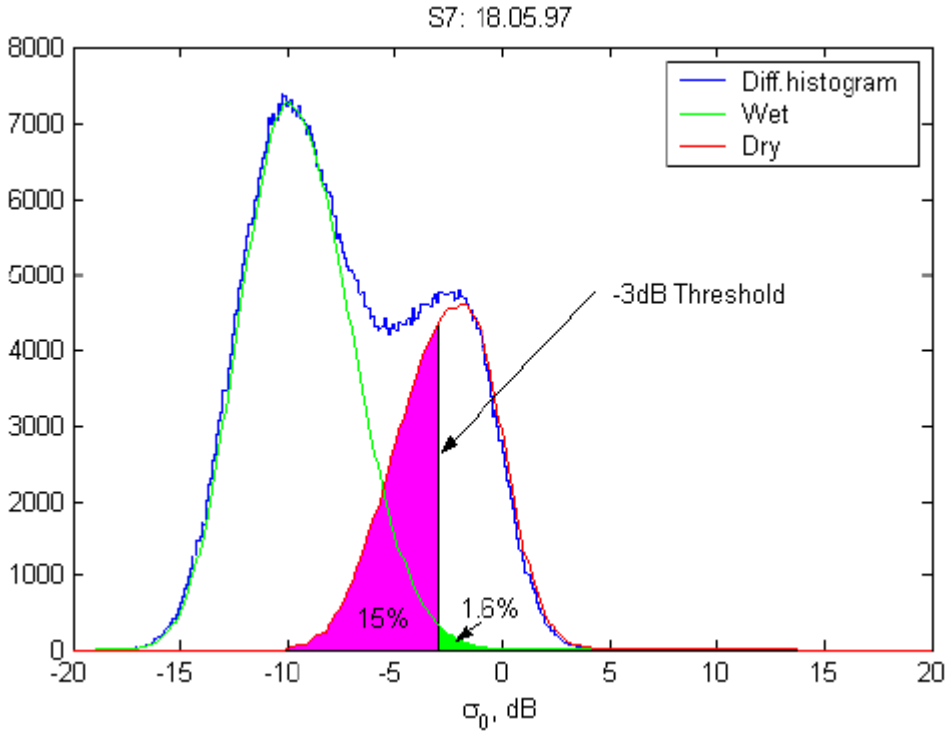

Figure 15: Error assessment. The difference image histogram is fitted with two distributions, representing wet snow and dry snow/bare ground. Error rates are calculated by estimating the areas below the respective curves from the threshold. Source: Malnes and Guneriussen (2002).

3.4.3.2 Using polarimetric data for snow cover monitoring

Fully polarimetric SAR data contain more information than single or dual polarization data, and have been used by several researchers in attempts to monitor dry and wet

snow cover. A big advantage of fully polarimetric SAR data is their capability to monitor total snow cover, not only wet snow. Martini et al. (2006) have developed a method that used fully polarimetric SAR data in C- and L-bands. While The L-band data were used to classify land cover, the C-band images were used for snow monitoring. It was found, that polarimetric decomposition can be used to identify snow-covered forests and that the polarimetric contrast between snow cover and bare ground in open landscape is too low for snow classification. On the other hand, snow in open landscape can be classified using supervised classification, but this procedure requires training samples. This led to forested and open areas being processed separately by Martini et al. (2006).

So the biggest drawback of using fully polarimetric data seemed to be the need for ground-truth data required to apply supervised classification algorithms. But Singh et al. (2014) have developed a new method, using ALOS-PALSAR data, which not only performs well in snow cover classification, but also does not require training samples. The only problem with this method is the low incidence angle of ALOS-PALSAR data, which leads to large layover-affected areas in mountainous regions.

Unfortunately, it is difficult to achieve fully polarimetric data, so in this paper I will be limited to the use of single polarization C-band data from ERS-2.

CHAPTER 4

Data, test area and methods

4.1 The test area

The area upon which I will attempt to observe wet snow cover must satisfy a few requirements in order to provide good conditions for developing and evaluating a SCA retrieval algorithm.

First of all, the terrain should be rather flat. This should help avoid topographic distortions and also the results should be easier to evaluate if altitude does not vary significantly inside a pixel (snow properties can vary significantly on short distances, if altitude does).

Since it is complicated to retrieve information from forested areas, the test area should contain some open ground or low vegetation. Also bogs or mires could pose a problem, because they are likely to appear as water bodies or wet snow due to the high amount of liquid water contained in them.

Furthermore, it is important to find an area where the snowpack is thick and stable enough during winter, so that so that the backscatter actually carries information about the snowpack. The snowpack's stability is important, because repeated freeze-thaw cycles lead to complicated stratification in the snowpack, which makes retrieving the snowpack information a bit more complicated.

Finally, there must be some ground-truth data available in the selected area so that the results can be evaluated.

These requirements are best satisfied in Scandinavian regions. The alpine regions satisfy the requirements of thick and stable snowpack and low or no vegetation, however, the terrain in these regions is so steep that radar instruments

cannot retrieve information from a large area. Eventually I have selected an area in southern Norway. The approximate location of the test area is shown in figure 16.

Figure 16: A map showing the approximate test area (blue rectangle). Background map: Kartverket, c2007

4.1.1 The test area description

Most of the Hardangervidda lies in altitudes above 1000 m a.s.l. , which makes it a mountainous region. However, the terrain is relatively flat. The few exceptions are some valleys and fjords. Probably the most significant are Måbødalen, Hjølmadalen and Simadalen. The only fjord that lies in the test area is Eidfjorden. The valley floors

are also covered with forests. Furthermore, there is quite a lot of lakes and bogs in the area, as well as a glacier, Hardangerjøkulen. These special types of land-cover will be masked and treated separately. Several of these lakes are, however dammed and used to produce electricity, so their extent may vary in the radar images and in the land cover map that will be used. The valleys and the fjord will also be accounted for.

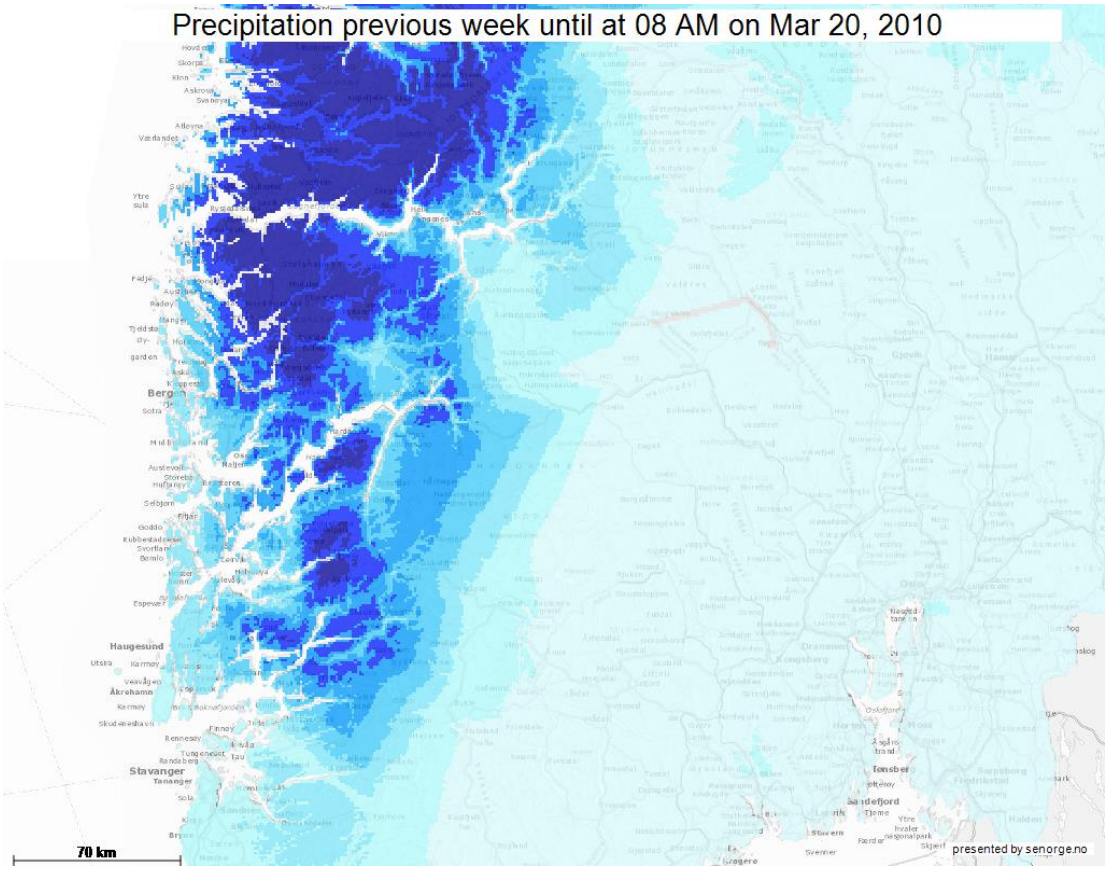

Figure 17: A typical winter week's precipitation over south Norway. Darker blue means more precipitation. Source: NVE (2013?)

The test area is also strongly influenced by the proximity of ocean, as the western part of the area receives significantly more precipitation. Ocean's influence should also result in higher winter temperatures in the western part, as well as it should be noticeable in snow wetness – snow should melt faster in the wetter and warmer parts. A typical winter's week precipitation in this part of Norway is shown in figure 17. It is clearly visible that the precipitation gets stronger as the clouds hit the mountains on the shore and then it gradually weakens. Figure 18 shows a typical seven days average temperature. It is obvious that the temperature drops

significantly in the central parts of the Hardangervidda plateau, compared to its eastern part.

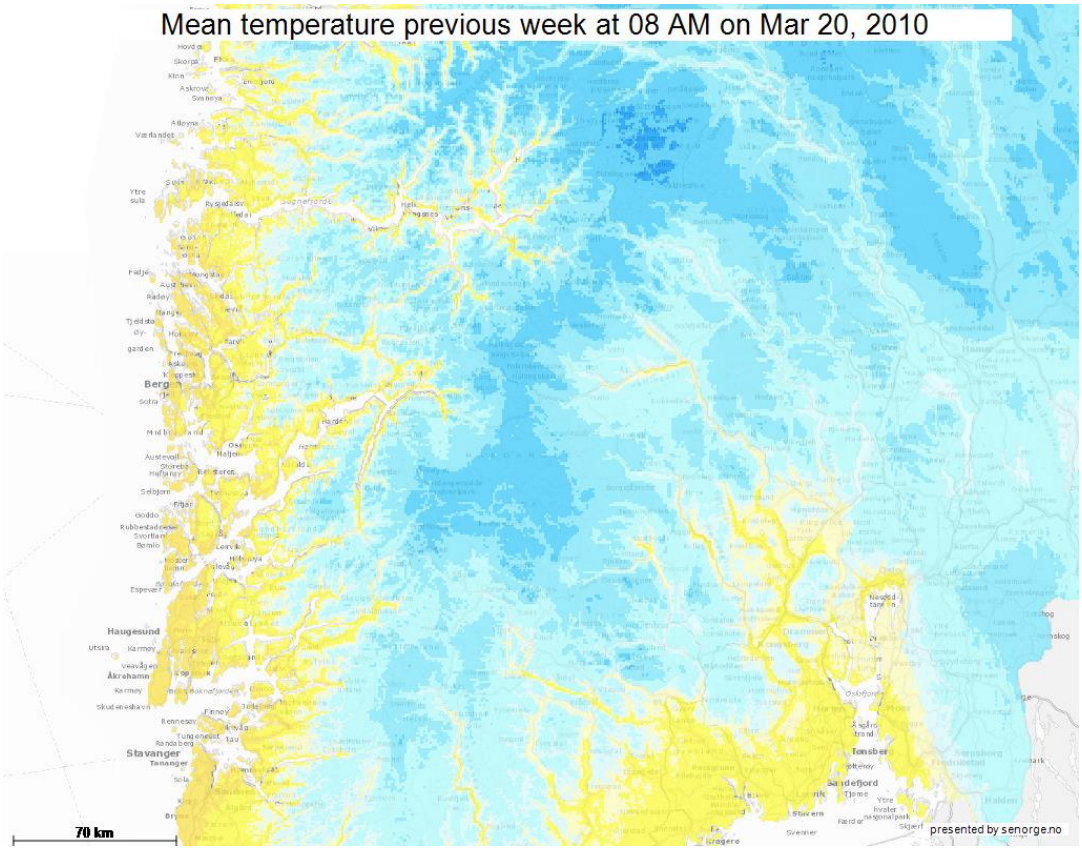

Figure 18: Average temperature over south Norway on a typical winter week. Shades of blue mean temperature below zero and darker means colder. Yellow means temperature above zero. Source: NVE (2013?)

All in all, the test area should provide enough bare ground with low altitude differences. The winter snow cover is also relatively stable here, and, except for the western part of the area and some of the valley floors, only starts melting on spring, so there should not be more freeze-thaw cycles which could cause complicated stratification in the snowpack.

4.2 Data

4.2.1 The satellite images

I have chosen to use data acquired by the ERS-2 mission, mainly because they are relatively easy to achieve for research purposes. Even though some other sensors, possibly in a different band and with polarimetric capabilities, could be more feasible

for this purpose, images from such sensors were not possible to obtain. Besides, it is important to conduct research even with data that do not seem to be the best for the purpose. Data used in this paper were provided by ESA. The choice of images depended on several factors.

The reference (snow-free) images had to be actually snow-free and, favourably, taken at a time when the soil was relatively dry. The dry soil requirement is important, because wet soil (e.g. soil containing large amounts of water) would have similar backscattering properties as wet snow. Finding images that satisfied both requirements was rather difficult, because Norwegian mountainous areas are usually not entirely snow-free before September. However, in this period it also rains a lot, so the soil is seldom dry. Furthermore, the first snowfall comes not very long after the last snow has melted. This is the reason why the reference image, taken in July 2010, will still probably contain patches of wet snow.

Nagler and Rott (2000) claim, however, that it is also possible to use images with dry snow cover as reference images. Using dry snow reference images eliminates the risk of wet soil occurring in the reference image. But due to the test area's diversity it was not possible to find an image entirely (or almost entirely) covered by dry snow. There are only a few days every year when the valley floors are covered by dry snow, and the chances of getting a satellite pass on one of the desired tracks during one of these days are very low.

The information about the reference images I have decided to use is summed in Table 5. As mentioned before, the reference image is likely to contain wet snow patches. There has also been some rain the week before each of these images was taken. However, the day before the image was taken, there has only been a little rain recorded over the test area, as seen in figure 19.

Date	Track	Orbit	Pass
19th July 2010	194	79707	D

Table 5: The reference image information.

It is also important for the reference and test images to have the same imaging geometry, so that the fold mask is the same for both images and the same area is depicted in them

The test images were chosen so that they would depict the test area during the snow melt season. I have therefore consulted the ground truth data when selecting these images. The information about the test images is summed up in table 6.

Date	Track	Orbit	Pass
13th April 1998	194	15579	D
5th May 2008	194	68184	D

Table 6: The test images information.

The April image should contain some wet snow, little snow-free ground and some dry snow. So does the May image, but it should contain much less amount of dry snow. These presumptions are based on ground-truth data used while selecting the images.

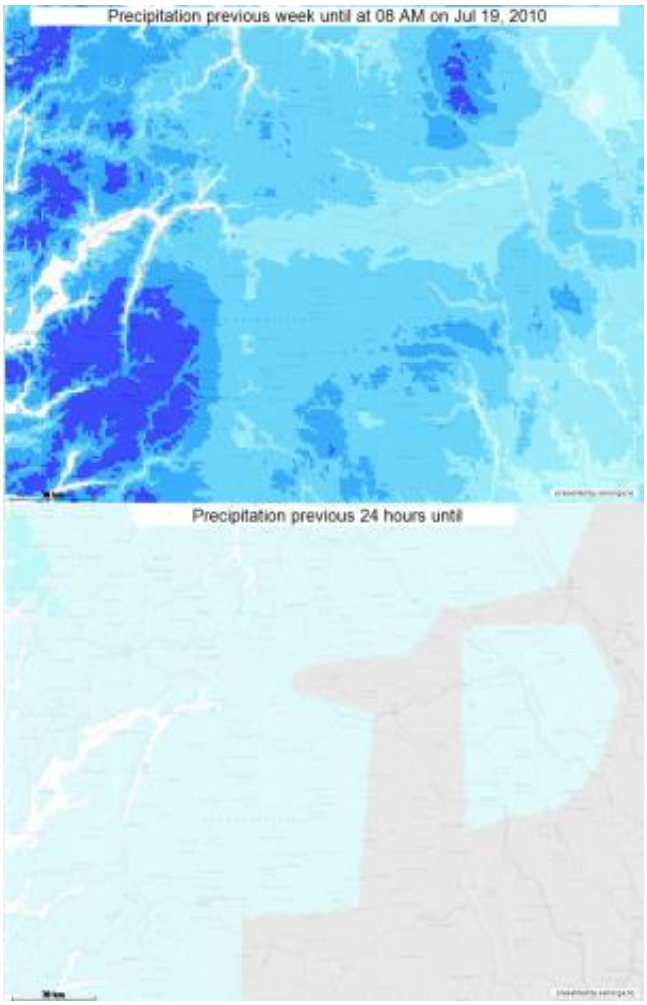

Figure 19: Precipitation over the test area the day/week before each of the reference images was taken. Source: NVE (2013?)

4.2.2 Ground-truth data

Ground-truth data concerning snow wetness, or snow properties in general, are very tricky to achieve. Many researchers elect to conduct a field campaign and then wait for satellite images acquired during the time of their field campaign. Such a field campaign must, however, be very thorough and it requires a lot of manpower to collect data from a large area during a relatively short period of time; collecting the data shortly before or after the satellite image acquisition is necessary, because snow wetness may change significantly in less than an hour (see chapter 3), especially in open landscape. Even if I ignore logistical problems (which could be avoided by choosing a different test area), I still lack the necessary manpower and equipment. Not mentioning the fact, that the ERS-2 mission was officially aborted in

2012, when I have barely started working on this paper. Field campaign is therefore out of the equation.

Sometimes optical data can be used, but it requires the optical image to be taken shortly before or after the radar image, and optical images cannot properly distinguish dry and wet snow, so they can only be used to verify the total snow-covered area. Also, the image must be cloud free, which is a condition that is hard to satisfy in Norwegian mountains during winter. However, when it comes to availability, this is probably the best option.

Automatic ground measurements of snow wetness are not operationally available in any of the regions I have considered when selecting the test area. Only some automatic measurements of snow depth are available in the test area, which can be used to very roughly compare the modelled and real snow extent. However, such measurements, taken from a single point, are not very reliable – the point where the measurement has been made, might be either a part of a small snow-free patch in otherwise compact snow cover, or a small patch of snow in an otherwise snow-free landscape.

However, the NVE has developed a model that computes various hydrological and meteorological statistics in a 1km x 1km grid. All the outputs of this model can be viewed online in a web browser at www.senorge.no and are also accessible via a WMS service. Altogether the models are called “seNorge” (seeNorway). Obviously, such a model is far from 100% precise, but it has been updated this year and its authors believe that it should be good enough. The old version of the model was subject to an intensive evaluation process (see Stranden, 2010), which helped in the update. After some electronic correspondence with a few NVE researchers, I have decided that this model is the best ground-truth I can get. Especially mr. Tuomo Saloranta has been very helpful, and also confirmed that the data from this model are probably the best choice for this purpose.

Therefore, I will be using data from the seNorge model to evaluate the results achieved in this paper. I also plan using the automatic snow-depth ground measurements in order to gain as much information about snow extent as possible, but the ground measurements are more of a supplement, and might not prove helpful at all.

4.2.3 Land cover data

Since radar backscattering may be strongly affected by some land cover categories even when a compact snowpack is present, it is good to handle some of these categories separately. This mostly concerns water bodies, forested areas and bogs and will be discussed further on.

Thanks to the EEA's (European Environment Agency) CORINE (Coordination of Information on the Environment) land cover project, many European countries have performed very detailed land cover mapping. Norway is, luckily, one of these countries and the land cover data were made freely available in vector format by the Norwegian Institute for Forests and Landscape. The smallest area covered in these data is 25 ha, which should be sufficient for the purpose of this paper.

4.2.4 DEM

A digital elevation model is required for SAR image processing, mainly to account for topographic effects on backscattering. Foreshortening can be corrected, while areas affected by layover and shadow should be masked out. Even though the algorithms used should not be affected by foreshortening, because they employ change detection.

For this purpose, I have purchased a 20 meter grid DEM by Kartverket – Norwegian national cartographic authority. This model should have a standard deviation between 2 and 6 meters and is probably the best option I had for this purpose, due to its combination of acceptable cost and reasonable level of detail and precision.

4.3 Methods

4.3.1 Pre-processing data

In order to be able to apply classification methods, the raw images, delivered in PRI (precision image) format, must be pre-processed, because the original data include such significant distortions and errors, that it is necessary to subject them to various corrections. These corrections are described in this chapter.

The images resulting from the pre-processing phase should be corrected for terrain induced errors, radiometrically normalized and speckle-filtered. For each of the raw images, an image in dB and another in linear values should be produced.

Similar corrections are commonly used when pre-processing SAR data. The common order of pre-processing steps is to apply radiometric corrections first, then speckle filtering and eventually terrain corrections. All of these corrections induce changes in the image, but are necessary for the image to be suitable for geocoding and to remove some radiometric errors, which are so significant that they make the raw images useless for classification or other analysis.

The aim of radiometric corrections is to modify the values received by the radar instrument, so that they correspond to the actual reflective properties of surfaces. Radiometric errors most commonly include missing lines or incorrect sensor calibration. When pre-processing digital remote sensing images in general, radiometric corrections should always be applied first, because geometric corrections sometimes, as well as speckle filtering change the original value of pixels, but radiometric corrections require unchanged values to be effective. Also, terrain corrections often rotate or otherwise geometrically transform the image, which could result in systematic radiometric errors (like missing lines) being transferred to multiple lines, thus making them more difficult to correct.

Radiometric corrections were carried out as the first part of pre-processing and were done using the latest version of ESA's NEST (Next ESA SAR Toolbox) software, which was 5.1, at the time of writing this paper. In order to use a PRI-formatted image in NEST's Terrain Correction operator, the image must first be radiometrically corrected. These corrections include correcting for antenna pattern gain, range spreading loss and analogue to digital convertor power loss. All these actions are performed by applying the Remove Antenna Pattern operator on the images.

After having applied the radiometric corrections, a 3x3 median speckle filter was applied to the image. The effects and drawbacks of speckle filtering are discussed in chapter 2.4.3. Because of the way speckle filtering works, we can only expect some loss of detail, but reducing speckle is more important and the loss of detail should not have significant influence on the final results.

Geometric corrections in this case include corrections of terrain induced errors, modelling the instrument's orbit and automatic geocoding. This process should not significantly influence the backscattering values recorded by the sensor.

Terrain induced errors are discussed in chapter 2.3. Orbit modelling is important to know the satellite's precise position at the time the image was taken, which in turn helps with precise geocoding. Geometric corrections are commonly applied as the last step of image pre-processing, because, they often include geocoding and resampling of the image.

All the necessary geometric corrections were carried out using NEST's SAR-Simulation Terrain Correction operator. This operator runs in three phases:

1. SAR Simulation:

    a. First, it generates a simulated SAR image using a given DEM, geocoding and orbit state vectors, and generates a model of SAR image geometry. The simulated image has the same size and resolution as the original image.

    b. Then, the position of each DEM cell inside the simulated SAR image is calculated.

    c. Finally, the program calculates the backscattering intensity sigma0, based on the backscattering model generated in step *a*.

2. Co-registration

    a. The simulated SAR image and the original SAR image are co-registered, and a function, which assigns every pixel from the simulated image to the position of a pixel in the original image, is created. The accuracy of co-registration depends, aside from other factors, on the number of control points. In my paper, I used the default number of control points, which is 200, and should be sufficient for a precise enough co-registration.

3. Terrain Correction

a. Traverse the DEM grid, and for each cell computes its position in the simulated SAR image.

b. The cell's position (step *a*) can then be found in the original SAR image with the help of the function produced in step *2a*.

c. The pixel value for the orthorectified image can then be obtained from the original SAR image using Interpolation.

The operator settings were applied as follows: In the SAR-Simulation tab of the operator's setting window, I chose both amplitude and intensity to be processed, selected the DEM I have obtained for this purpose and checked the 'Save Layover-Shadow Mask' checkbox. I have kept the default values in the GCP-Selection tab, because the recommended number of ground control points should be sufficient for precise geocoding of a standard ERS image, and checked 'Apply radiometric normalization' and 'Save Sigma0 band'. The Sigma0 band will be used for image classification. The radiometrically normalized Sigma0 band reduces the effect of local incidence angle on backscattering (step *1c* in the SAR Simulation Terrain Correction operator), which makes the final backscattering correspond better to the actual backscattering properties of the surface.

The SAR-Simulation Terrain Correction operator also geocodes the images, so I have chosen to have the results geocoded in WGS84 projection.

For more details on the tools used in this part of the pre-processing phase, please refer to ESA (c2000-2014).

As mentioned before, all of these corrections are generally used to help achieve a better result, especially radiometric corrections, corrections of terrain-induced errors and geocoding are necessary to achieve an image that is suitable for further processing, and the changes induced in the images by these corrections are considered negligible, especially when compared to the significant errors that can be found in the original images. Also, this pre-processing procedure corresponds to that used by other authors.

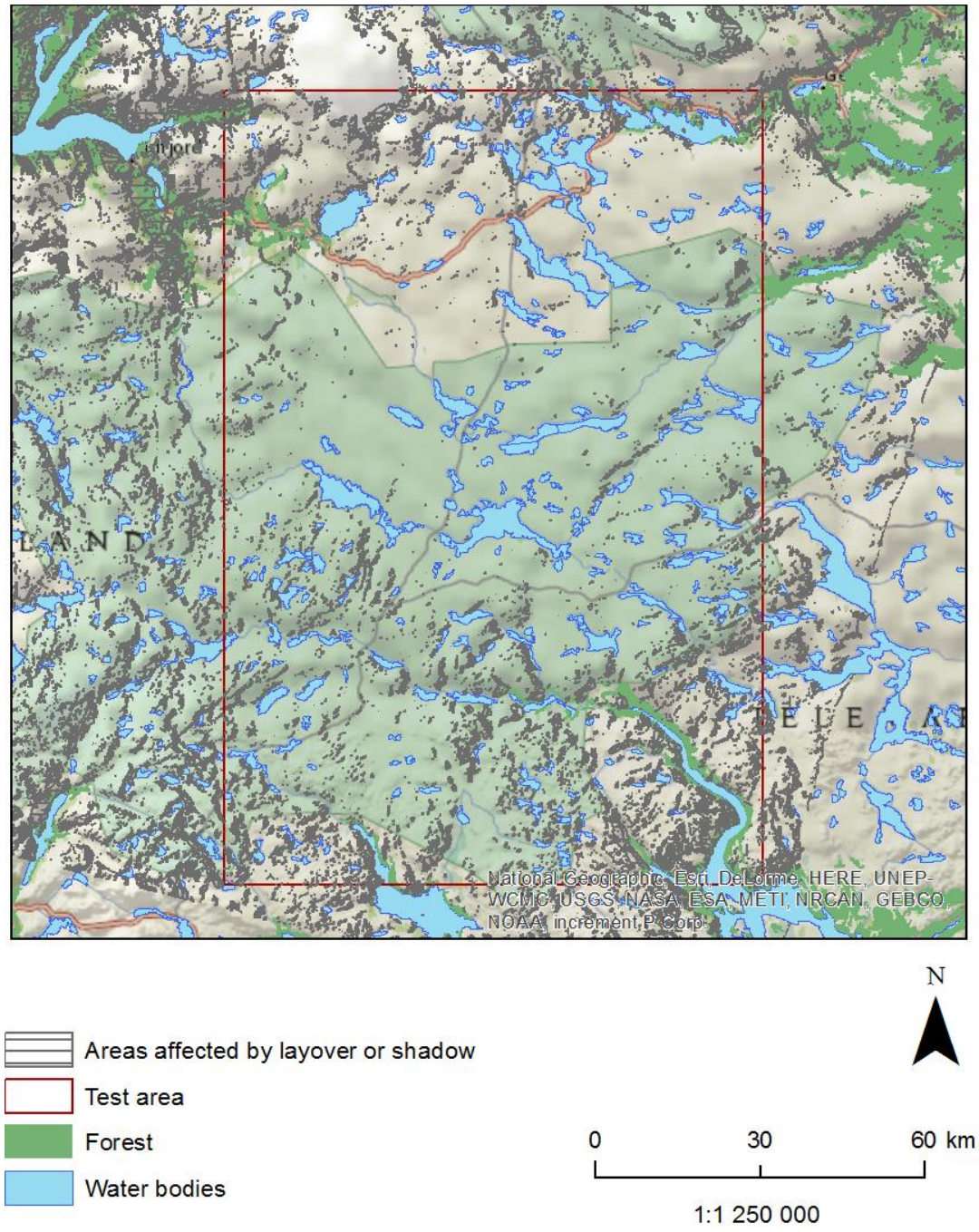

Figure 20: The exact test area and masks of water, forest and layover/shadow. Background map: National Geographic, Esri, DeLorme, HERE, iPC, NRCAN, METI (2014?).

Finally, I created a new Sigma0 band in dB by using NEST's Linear to/from dB operator. The resulting image contains a band in dB, another band in linear units and a band of layover and shadow mask. The last step then was to export the bands images to GeoTIFF format, so that they can be opened in ArcMap for further processing. I did not need all the bands to be exported, only the σ_0 band in dB and in linear units, and the layover/shadow mask.

After having completed the above steps, the next part of pre-processing took place in ArcMap 10.1. First of all, I had to address the issue of performance, because the images exported from NEST were very large and my computer was unable to work with them efficiently. This is why I decided to only work with a portion of the total area covered on the satellite images. The final test area is depicted in figure 19.

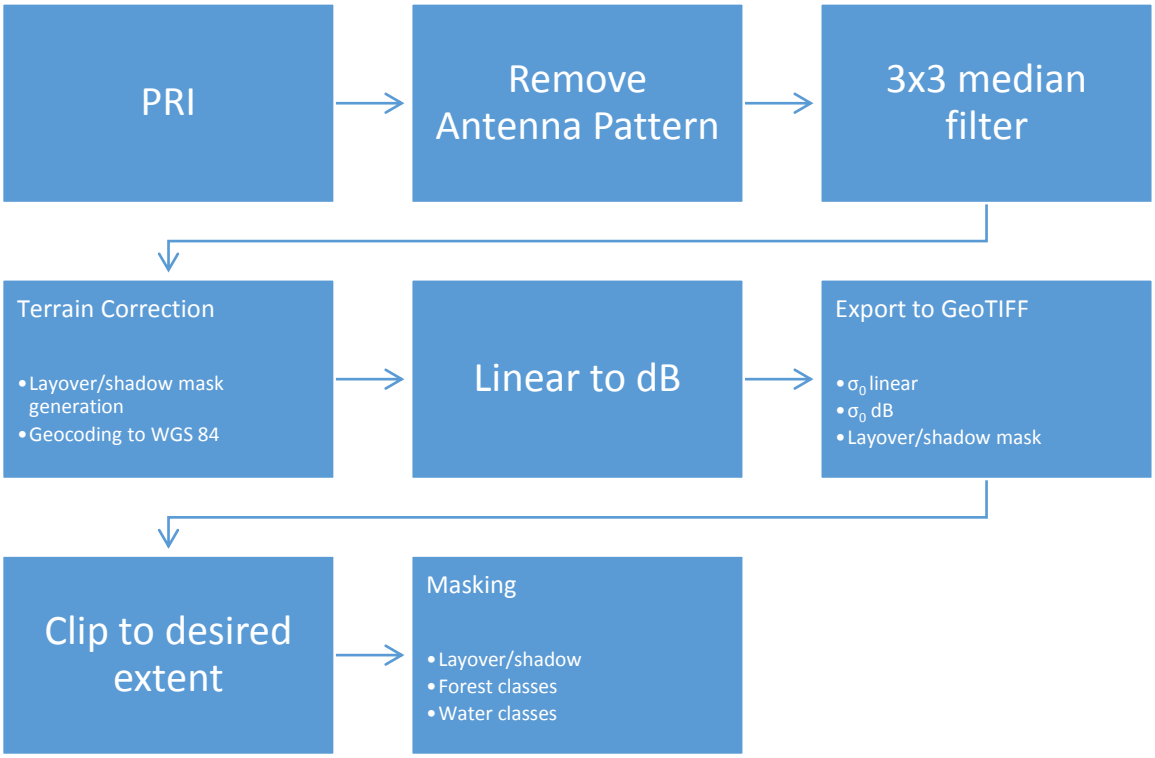

Figure 21: A flowchart of the pre-processing phase.

Once the images have been clipped, I have masked out areas affected by layover and shadow, and then forest and open water areas. Layover and shadow mask was derived during terrain corrections in NEST, while forest and water mask were derived from CORINE land cover dataset. Forest mask includes areas that have been classified as borad-leaved, coniferous or mixed forest while the water mask includes rivers, water bodies, coastal lagoons, estuaries and sea and ocean. Also the water and forest mask can be seen in figure 20, as well as layover and shadow.

After having performed all the pre-processing steps on all three images, I had a set of six images – an image in linear units and another in dB for each date. All images are geometrically and radiometrically corrected and masked for areas I

wanted to leave out of the classification process. The pre-processing phase is simply depicted in a flowchart in figure 21. The resulting images are ready to be applied as input in a snow wetness classifiaction algorithm.

4.3.2 The classification algorithm

In this paper, I have chosen to classify wet snow by using the algorithm developed by Malnes and Guneriussen (2002) (see chapter 3.4.4.1.3 for further details on this algorithm) and compare its performance with data in linear units and in dB. The reason to base my work on a relatively old paper, was the fact, that this is the newest paper that has made significant progress with non-polarimetric data, and also that many other authors base their work on the work of Malnes and Guneriussen (2002), attempting to resolve the issue of classifying dry snow. However, as the amount of relatively new articles described previously in this paper suggests, the topic of wet snow monitoring with single polarization C-band SAR is still active, in spite of the fact that it seems to have hit a dead end and many of the papers are still based on older techniques. C-band SAR can still provide valuable information about snow cover, and there are currently no plans of launching an instrument with better parameters for snow monitoring, even though there is an ongoing research on this topic, like the aforementioned CoReH2O project, so trying to improve current methods is still an attractive research topic.

In order to be able to use data in linear units, the algorithm must be slightly modified. When working with decibel data, I need to calculate the difference between the reference image and the image of interest. However, with data in linear units, a ratio image must be calculated (reference image/image of interest, see Bartsch (2007)).

Another difference between classifying data in dB and in linear units is the threshold value. While for the images in dB, the soft threshold I have used is centred at -3 dB, in case of data in linear units the threshold is centred at 2. These are the thresholds used by Malnes and Guneriussen (2002) and Bartsch (2007) for data in dB and linear units, respectively. The images were classified using ArcMap 10.1 and its Raster Calculator tool. The classification of images in dB was conducted using formula 7 (see chapter 3.4.4.1.3). I have chosen to set the *a* parameter value to 1 (both for classification of dB and linear data), because it does not seem to have any significant effect on the classification results.

The classification formula had to be slightly modified for linear data, for several reasons. First of all, the threshold value is different. Also, with data in dB values, values lower than threshold are classified as wet snow, while with data in linear values, pixels with value higher than threshold are classified as wet snow. These two issues can be solved by simply changing the threshold value in the formula and by flipping the sign before the hyperbolic tangent. The result of this modification is formula 8.

$$\mathbf{8}: F(x) = 50 + 50 * \tanh[a * (x - 2)] \ \%$$

The final issue that needed to be addressed is slightly bigger and has several possible solutions. For the classification function to result in a value of 0, the parameter of the hyperbolic tangent must be slightly lower than -19. However, the linear values are always positive, which means that the classification never reaches 0 and would never classify a pixel as entirely snow free.

To solve this problem, I needed to make the classification curve be able to reach both extreme values (0 and 100) within the given dataset. A possible solution would be to use a number larger than 1 for parameter *a*. I have decided not to choose this path, because it would make the classification curve so steep that using a “soft” threshold and sub-pixel classification would no longer make sense, because the results would be nearly identical to classification with a “hard” threshold. It would also make the classification results of dB and linear values incomparable, as well as it would affect the possibility of retrieving dry snow from the classification results.

Eventually I have decided to not change the classification function, and rather reclassify the values that are close to 0 or 100. The result is, that values lower than 5 are reclassified to 0 and values higher than 95 are reclassified to 100. This procedure maintains comparability, if applied on all linear and dB datasets, and also minimizes loss of information gathered by the sub-pixel classification process, as well as it maintains the possibility to classify dry snow.

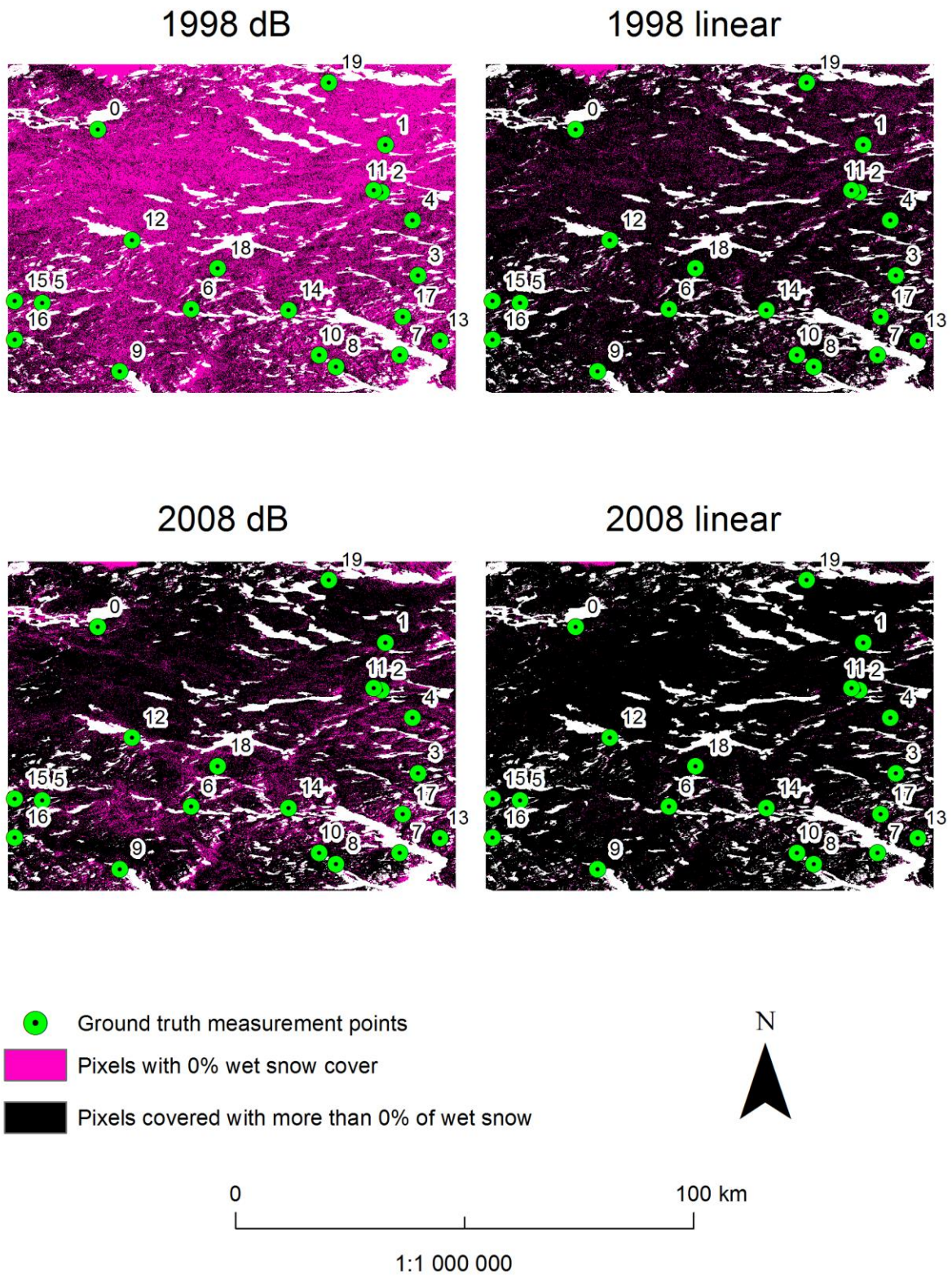

Figure 22: 0% wet snow mask (in pink). Black pixels contain more than 0% of wet snow, white pixels represent areas where no data could be achieved due to topographic effects or water/forest presence.

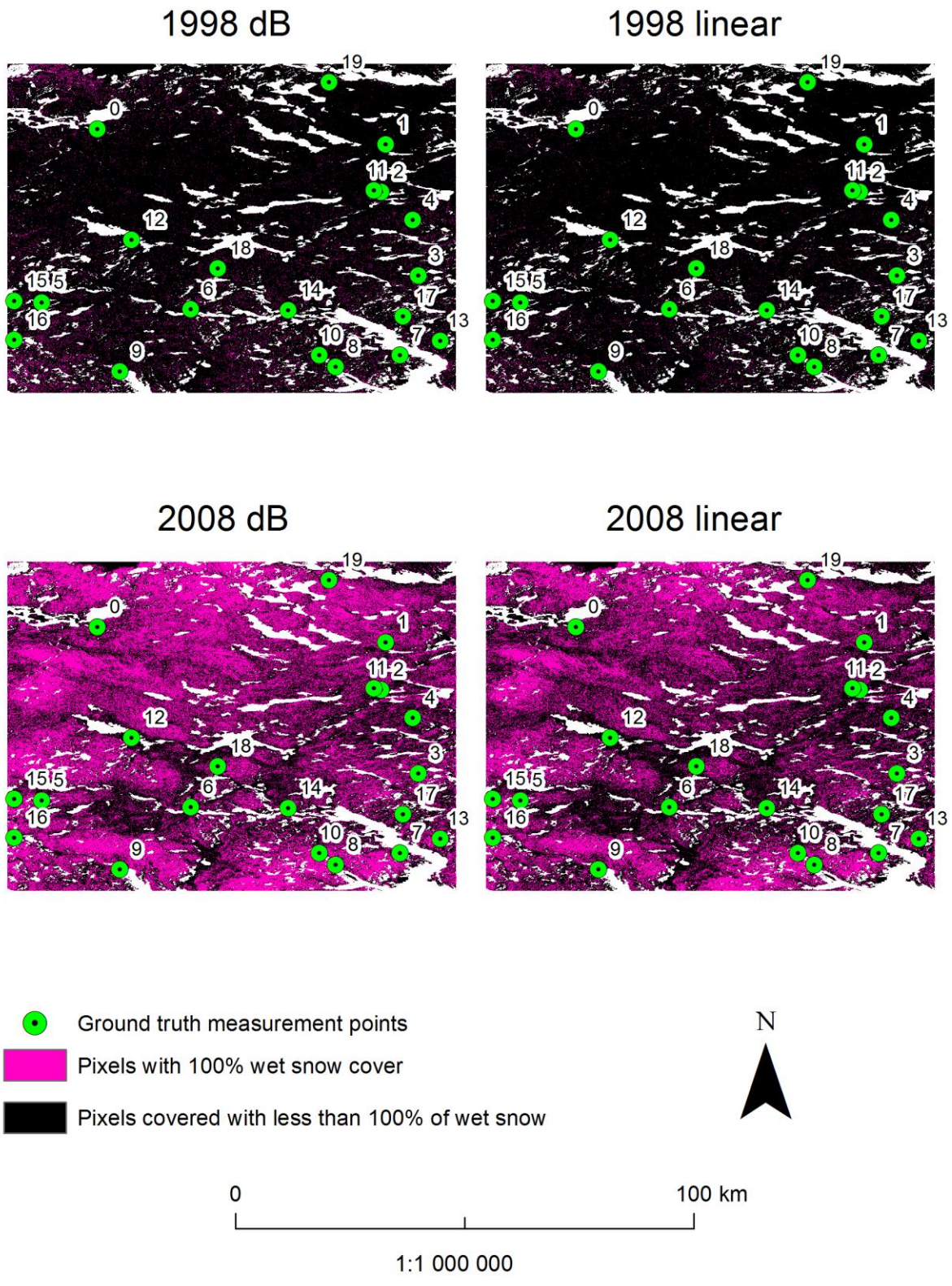

Figure 23: 100% wet snow mask (in pink). Black pixels contain less than 100% of wet snow, white pixels represent areas where no data could be achieved due to topographic effects or water/forest presence.

The final phase of classification where dry snow is being identified, can be affected by this modification. However, this is not necessarily a bad thing, because it eventually leads to an increase in the number of pixels classified as dry snow or bare ground, and Malnes & Guneriussen (2002) have found, that their algorithm falsely classifies many pixels as wet snow, while they should have been classified as dry snow or bare ground. So this modification might, in fact, help improve the overall classification accuracy.

After having performed the reclassification, the final step is finding dry snow. As a prerequisite for this part of the classification process, I needed to create masks of snow-free pixels (or pixels containing less than 5 % wet snow before the reclassification), as well as a mask of pixels with 100 % wet snow (more than 95 % before reclassification). These masks are presented in figures 22 and 23.

In order to identify pixels that contain dry snow, the median altitude of pixels containing 100 % wet snow is calculated. Then, pixels lying above the median altitude and not containing any wet snow, are classified as dry snow. Table 7 summarizes the median altitude for both images in both dB and linear units. The median altitude was calculated in R, using the RGDAL library and its readTIFF function. The table contains values for both images in linear and dB values, processed by the modified algorithm. In order to maintain close comparability between datasets in dB and in linear values, I had to use the same parameter *a* while processing both datasets (*a* = 1 in this case, because using a smaller value would result in linear data getting even further from zero). I have also processed the datasets in dB using the original classification procedure as suggested by Malnes & Guneriussen (2002), while also processing it with the modified algorithm and the parameter value equal to 0.5, so that the impact of the algorithm modification can be examined.

From this table, we can presume that the highest amount of pixels classified as dry snow will occur in the dB image from 1998, classified with a = 0.5. The other image with a very low median altitude of 100% wet snow will probably contain much fewer pixels that will enter the process of masking by altitude, because it is the only case where I did not apply the reclassification rule of changing the values lower than 5 to 0, thus maintaining the original procedure suggested by Malnes & Guneriussen (2002).

	dB a=0.5, orig	dB a=0.5	dB a=1	Linear a=1
1998/04/13	1258	1261	1268	1264
2008/05/05	1369	1278	1265	1273

Table 7: Median altitude of pixels containing 100% wet snow.

After having calculated the median altitudes, all pixels lying above the median altitude and classified as no wet snow, are reclassified as dry snow. Then, the final version of the classified image can be produced by combining the results of wet and dry snow classification. The entire classification process is described in a flowchart in figure 24. The results are presented and discussed in the following chapter.

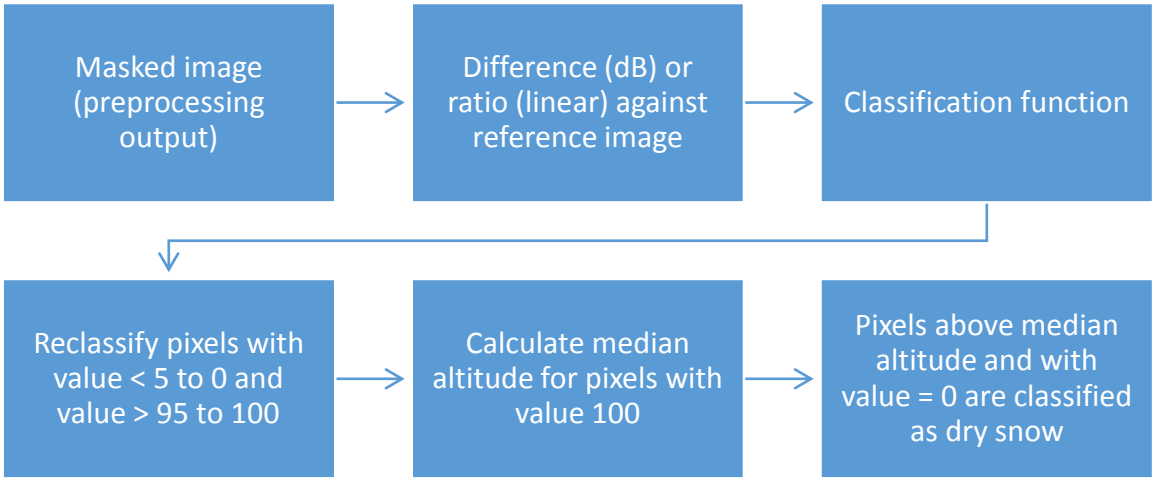

Figure 24: The classification process

CHAPTER 5

Results & discussion

Figures 25 and 26 show the snow maps resulting from the classification process described in the previous chapter. A total of four variations of the classification algorithm were used, and the results vary significantly, depending on the procedure.

Error assessment was carried out by generating 20 random points inside the test area, and then comparing the values of pixels lying on these points. The seNorge model served as the reference dataset. Due to a significant difference in spatial resolution between the classified ERS images and the model's output (25 m vs. 500m), I found it appropriate to not compare a single pixel from the classified image against a single pixel in the reference image. Instead, I decided to create a 200m buffer zone around each test point, and use the most frequent value inside this buffer zone as the classified value. This procedure was carried out for each of the eight classified images and the results can be seen in tables 8 and 9.

Another way of error assessment is visual comparison of the two datasets (classified image and seNorge's model output), which is a procedure that does not offer any quantifiable result, but can provide a nice overview of the situation. The model outputs can be seen in figures 27 and 28.Unfortunately, these images are taken from an external source, so I had very little control over their appearance, so they are missing important things like graphical legend or ground truth control points.

Upon visual inspection, the first thing to notice is, that the top-left image in figure 25, which was classified using the modified algorithm and $a = 1$, contains a lot of bare ground pixels, which probably should have been classified as either wet or dry snow. This is most likely caused by the parameter value, because higher parameter value reduces the amount of intermediate values in the classification result. This leads to more pixels being classified as either 100% wet snow or bare

ground. Another factor that probably has contributed to this, is the reclassification of values below 5 and above 95, which lead to an even higher number of pixels being classified as zero (bare ground).

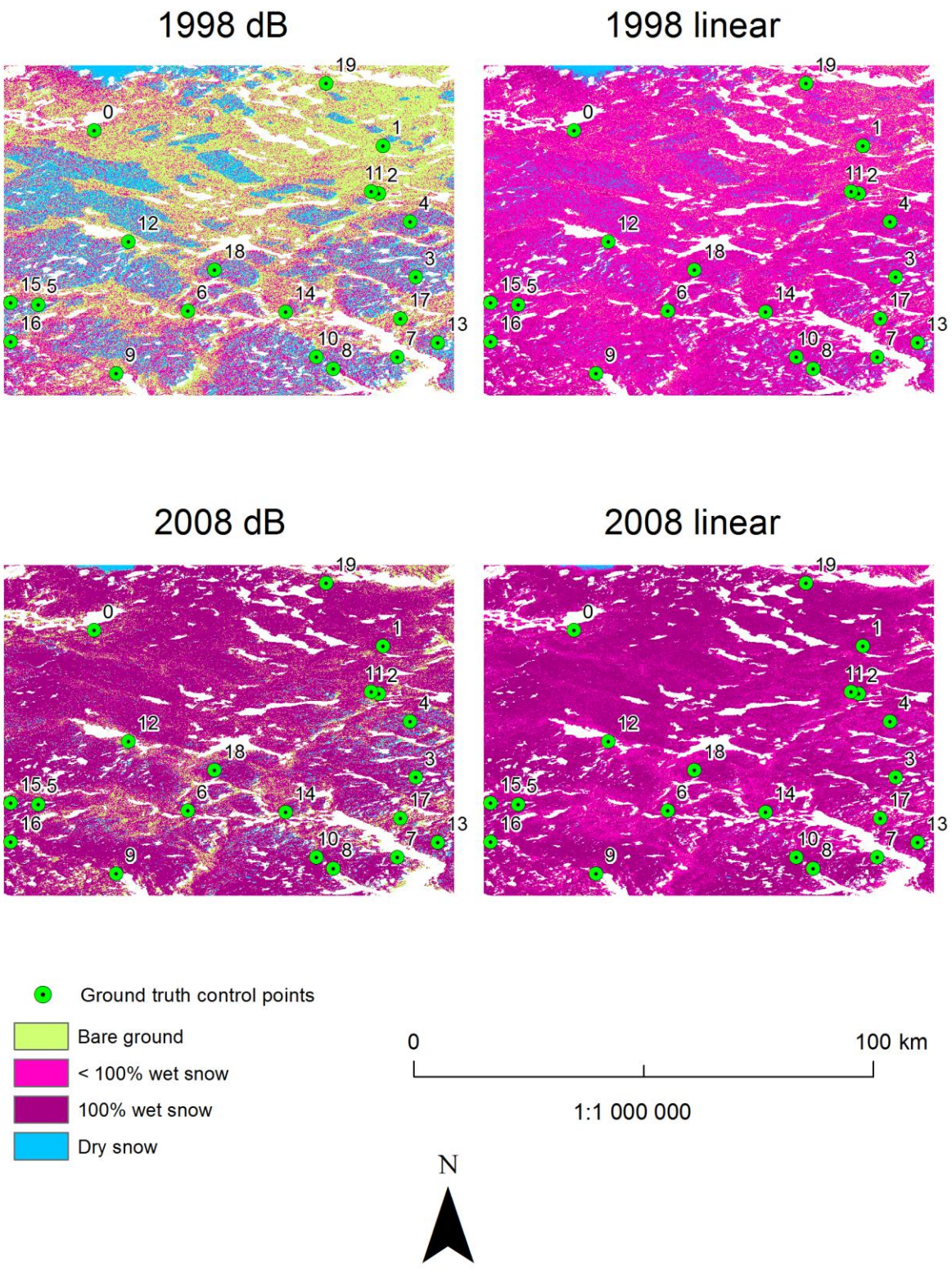

Figure 25: Classification results for the modified algorithm with dB and linear data for a = *1*

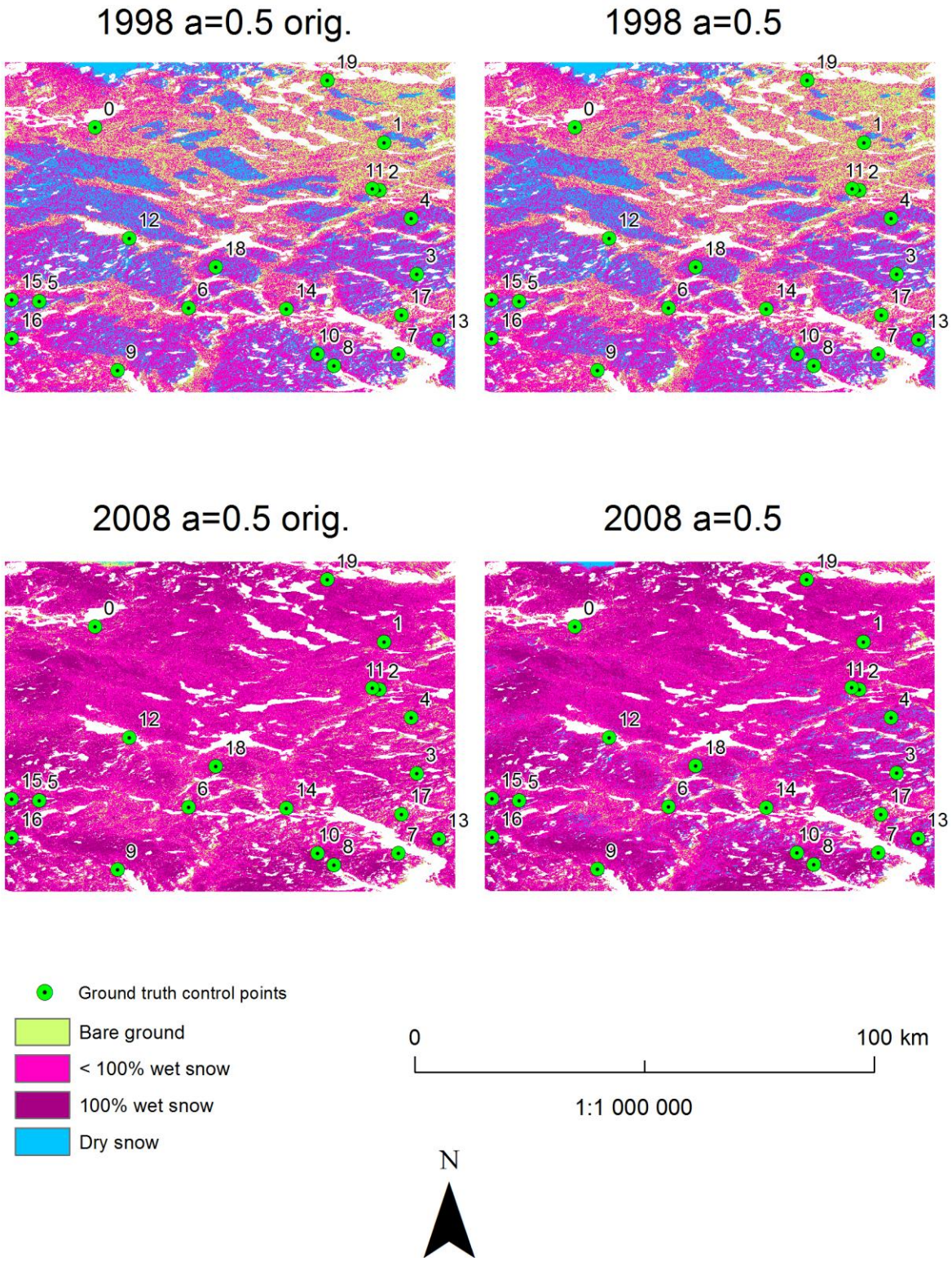

Figure 26: Classification results for the original and modified algorithm with dB data and a = *0.5.*

In the other two images from 1998, which were classified from data in dB, we may notice a decrease in the number of pixels classified as bare ground, but

also fewer pixels classified as dry snow. This indicates, that the parameter value probably had stronger influence on wrongly classifying many pixels as bare ground, than the reclassification of values close to 0 or 100.

Also, all the 1998 dB images contain much more wet snow than they should, according to the seNorge's model output. Because other researchers have found that thresholding techniques are quite reliable in classifying wet snow, I believe that this is probably caused by the difference in spatial resolution of the two products. Relatively coarse spatial resolution of the reference model may lead to ignoring small or narrow areas of wet snow in the output, which could explain these differences between the classified images and the ground truth image. But this still suggests, that in these images, we can expect some dry snow misclassified as wet snow. Otherwise, the general spatial distribution of dry snow is similar in all of the classified images and the reference ground truth image, which can be observed especially in the top left corner of the classified images, which roughly corresponds to the arc of dry snow in the ground truth image.

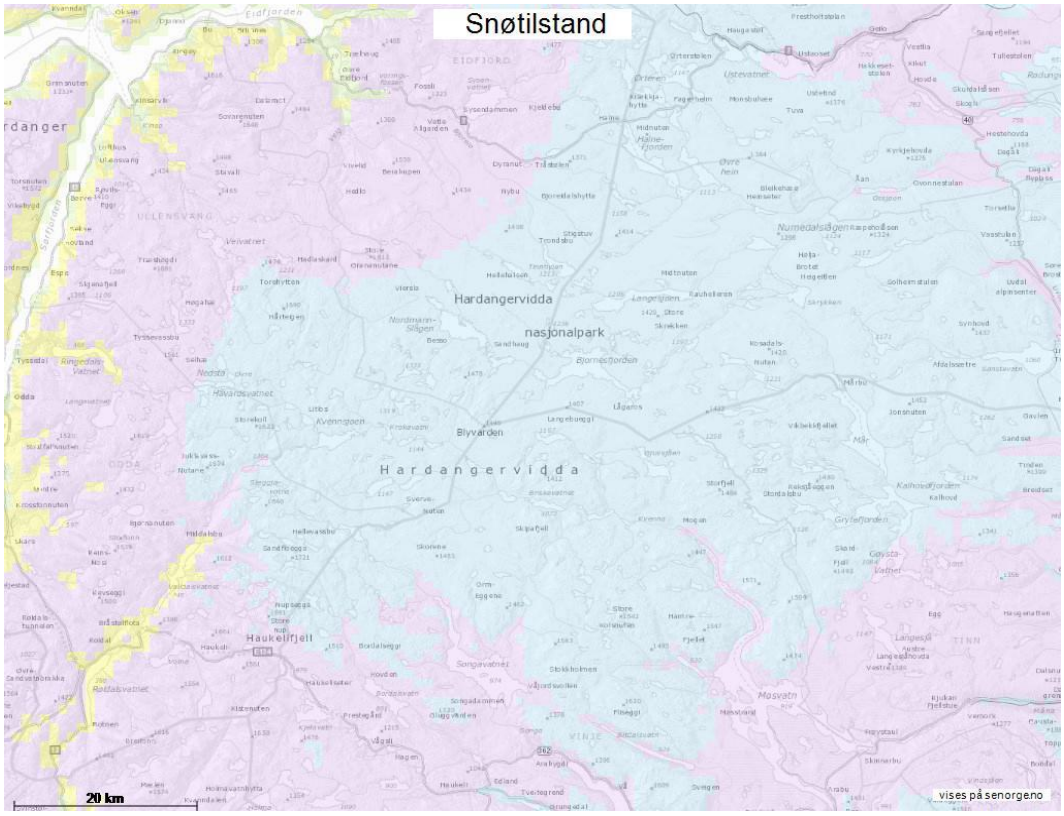

Figure 27: Snow wetness on 13th April 1998 according to NVE. Green colour indicates no snow, yellow colour indicates very wet snow (above 10% liquid water content), purple indicates wet snow (2-9 liquid water) and blue colour indicates dry snow (less than 2% liquid water content) Source: NVE (2013?)

Table 8 confirms what visual inspection suggested – in the 1998 dB images, wet snow is almost always classified correctly, while dry snow is often misclassified as wet snow or bare ground. The possible reasons for misclassifying dry snow as bare ground were discussed earlier. Misclassification of dry snow as wet snow might have been caused by different time of acquisition of the data, as especially during the melting period, snow may freeze over night, and then start melting again during the day. SeNorge's model output is calculated to 8AM, while the 1998 image was taken around 10:30 AM, which might have caused some difference in snow wetness. Also, the aforementioned coarse spatial resolution of the ground truth model output may have caused smaller areas of wet snow to be ignored, and classified as dry snow.

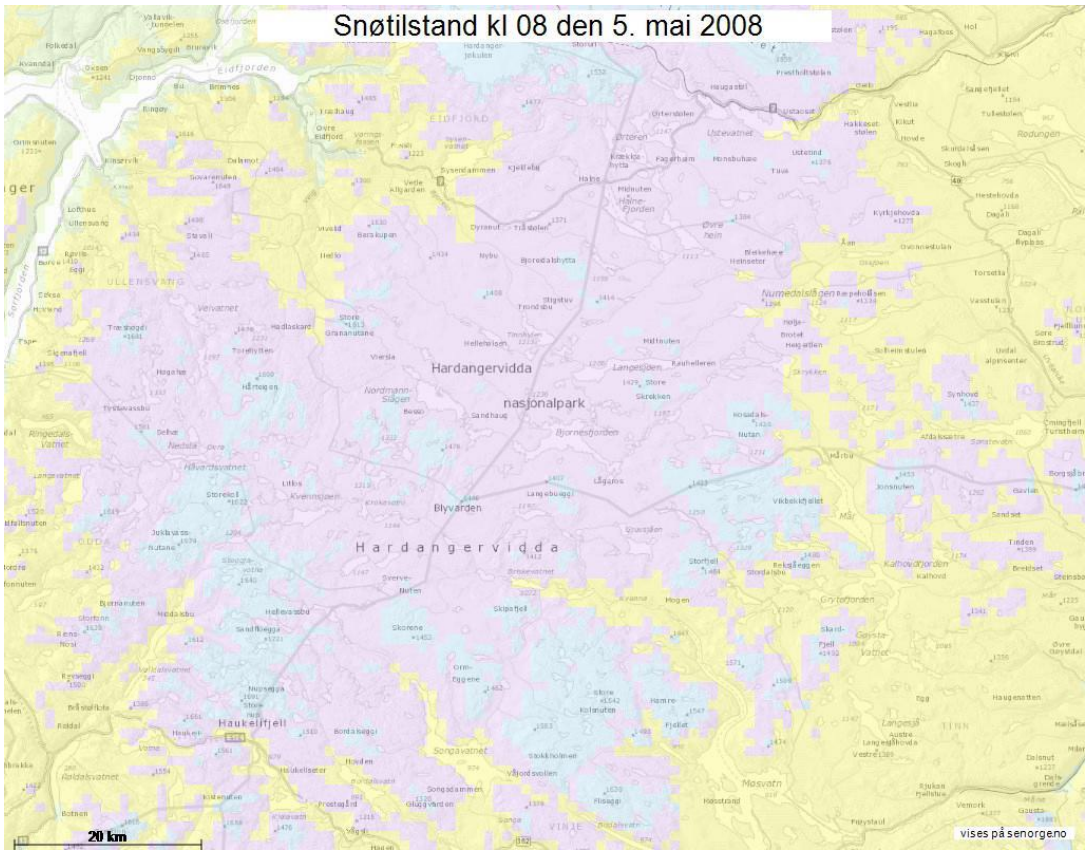

Figure 28: Snow wetness on 5th May 2008 according to NVE. Green colour indicates no snow, yellow colour indicates very wet snow (above 10% liquid water content), purple indicates wet snow (2-9 liquid water) and blue colour indicates dry snow (less than 2% liquid water content) Source: NVE (2013?)

The image from 1998, classified from linear values, contains hardly any pixels classified as dry snow or bare ground. Even though the spatial distriubution of dry snow pixels is similar to that of other 1998 images, the density of dry snow pixels is

still very low. Also the data in table 8 confirm very frequent cases of dry snow being misclassified as wet snow. These errors are most likely caused by very low amount of pixels classified as 0 or 100 compared to images in dB. This can also be seen in figures 22 and 23.

This problem could not be observed in such a big scale on the linear image from 2008, mostly because there is very little dry snow in the 2008 scene. But still, when compared to the dB images and the ground truth image, there is much fewer pixels classified as dry snow in the linear image than in the others. These results suggest, that images in linear values are not suitable to be used in this algorithm, even though the algorithm has been modified to suit linear data.

Ground truth point number	real snow status	1998 a=0.5	1998 a=1	1998 a=0.5 orig.	1998 linear
0	dry	dry	dry	dry	wet
1	wet	wet	ground	wet	wet
2	wet	wet	ground	wet	wet
3	dry	ground	ground	ground	wet
4	dry	wet	ground	wet	wet
5	dry	wet	wet	wet	wet
6	dry	wet	dry	wet	wet
7	dry	dry	dry	dry	wet
8	dry	wet	ground	wet	wet
9	dry	wet	ground	wet	wet
10	dry	dry	dry	dry	wet
11	dry	ground	ground	ground	wet
12	dry	wet	dry	wet	wet
13	dry	wet	ground	wet	wet
14	dry	ground	ground	wet	wet
15	dry	wet	ground	wet	wet
16	wet	wet	ground	wet	wet
17	dry	ground	ground	ground	wet
18	dry	dry	dry	dry	wet
19	dry	wet	wet	wet	wet

Table 8: Classification error assessment for the 1998 image

The 2008 scene was covered mostly by wet snow, with some areas of dry snow. The best results were achieved with the modified algorithm applied on data in dB values. Both results of the modified algorithm, with a = 0.5 and 1, show wet snow over most parts of the test area, and some areas of dry snow, which corresponds well to the ground truth image. Also the random point error assessment shows good

results. However, the dry snow areas are still very sparse, just like in the 1998 images, and the only random point that was actually lying on dry snow, was misclassified as wet snow. The image that was classified with *a* = 1 also contains some bare ground pixels. These are very sparse and are located in areas where the ground truth image reports very wet snow (more than 5% of liquid water content), so these bare ground pixels might in fact be classified correctly, and are not visible in the ground truth image due to its spatial resolution. This possibility seems more likely than misclassification, because classification of very wet snow should be reliable with this method.

The 2008 scene classified with the original algorithm contains hardly any dry snow pixels, and looks very similar to the 2008 linear image. These two images also contain the same misclassification of wet snow.

Ground truth point number	real snow status	2008 a=0.5	2008 a=1	2008 a=0.5 orig.	2008_linear
0	wet	wet	wet	wet	wet
1	wet	wet	wet	ground	ground
2	wet	wet	wet	wet	wet
3	wet	wet	wet	wet	wet
4	wet	wet	wet	wet	wet
5	wet	wet	wet	wet	wet
6	wet	wet	wet	wet	wet
7	wet	wet	wet	wet	wet
8	wet	wet	wet	wet	wet
9	wet	wet	wet	wet	wet
10	wet	wet	wet	wet	wet
11	wet	wet	wet	wet	wet
12	dry	wet	wet	wet	wet
13	wet	wet	wet	wet	wet
14	wet	wet	wet	wet	wet
15	wet	wet	wet	wet	wet
16	wet	wet	wet	wet	wet
17	wet	wet	wet	wet	wet
18	wet	wet	wet	wet	wet
19	wet	wet	wet	wet	wet

Table 9: Classification error assessment for the 2008 image

In the case of 2008 data, both visual inspection and random point error assessment suggest, that the best results were achieved by applying the modified

algorithm on dB data. The value of parameter *a* plays an important role in classifying dry snow and bare ground, and slightly better results were achieved with $a = 1$.

Data from 1998 were best classified by the modified algorithm and the original algorithm, both with $a = 0.5$. The modified algorithm with $a = 1$ achieved nearly the same error rate in random point error assessment, but clearly misclassified many pixels as bare ground.

The most reliable results were achieved in classifying wet snow – only very few pixels that contained wet snow were misclassified. This is not very surprising, since the classification algorithm is derived from algorithms that have proven their capability in classifying wet snow.

CHAPTER 6

Summary

I have examined several algorithms for classifying wet snow from SAR data. One of these algorithms was modified and applied on SAR data in different units. The original algorithm was also applied on the same datasets, and the results were compared.

The best classification results were achieved with the modified algorithm and dB data, even though the original algorithm performed nearly just as well. The modification consists of reclassifying results of sub-pixel wet snow classification so that values < 5 become 0 and values > 95 become 100.

The attempt to achieve better classification results, by modifying the algorithm so that it can process data in linear values, failed. Probably because the linear images classified with the wet snow sub-pixel classifier have too many intermediate values and not enough extremes indicating either bare ground or 100% wet snow. These extreme values are crucial for being able to distinguish bare ground from dry snow. The classification results contained only a few dry snow pixels, and while the spatial distribution of these pixels was correct, there was still much more wet snow pixels in the areas that should have been classified as dry snow. In order to be able to use linear data for classifying dry snow, a different approach should probably be considered.

The best results were achieved with classifying wet snow. Even though in some cases (1998 dB with a = 1) pixels that probably should have been classified as wet snow were classified as bare ground, either because of the temporal difference between ground truth data (8AM) and the satellite image (10:30 AM), or due to the fact that parameter a = 1 results in more pixels being classified as extreme values.

Wet snow extent seems to be overestimated in the 1998 images, and it looks like some areas should have been classified as dry snow. This might have been cause by the difference in spatial resolution between ground truth data and the classified image, as the wet snow areas are not very big, so they may have been classified as dry snow in the ground truth model output, because most of the pixel area was covered by dry snow.

Dry snow classification was not so successful. The spatial distribution of dry snow pixels roughly corresponds to ground truth, but dry snow areas still contain a lot of wet snow pixels (this issue is much less significant in dB data). In the case of dB data, this may have, again, been caused by the difference in spatial resolution between ground truth and the classified image.

The value of parameter *a* in the classification function seems to have a significant effect on dry snow classification, which can be seen very well on the example of 1998 dB image. The image classified with $a = 1$ contains a lot of bare ground pixels (that should have been classified as snow), but also much more dry snow, which, in turn, is correct. However, on the 2008 dB images, it seems that the image with $a = 1$ has better results than the image with $a = 0.5$. But on the 2008 image there is very little dry snow, so this may be misleading. I have not been able to find any lead that would suggest which parameter value is better for which use case, so this requires further research.

REFERENCES

BARTSCH, A., et al. 2007. Monitoring of spring snowmelt with Envisat ASAR WS in the Eastern Alps by combination of ascending and descending orbits. *Proc. Envisat Symposium.*

DOBROVOLNÝ, P. 1998. *Dálkový průzkum Země. Digitální zpracování obrazu.* Brno, Přírodovědecká fakulta Masarykovy univerzity, Katedra geografie. ISBN 80-210-1812-7.

DOLEŽAL, E., POLLAK, T. 2004. *Vlastnosti sněhu* [online]. [quoted 2013-05-20]. Available from URL: <http://ekologie.upol.cz/ku/mat/zhoek>.

ENGEN, G. et al. 2003. *New approach for Snow Water Equivalent (SWE) estimation using repeat pass interferometric SAR*. Proceedings IGARSS03, Toulouse, France, July 2003

ESA. c2000-2014. *Next ESA SAR Toolbox* [online]. [quoted 2014-08-24]. Available from URL: <https://earth.esa.int/web/nest/home>

FERRETTI, A. et al. 2007. *InSAR Principles: Guidelines for SAR Interferometry Processing and Interpretation.* The Netherlands, European Space Agency

FINSLAND, W. 2007. *Vurdering av mulighetene for kartlegging av snøskred med fjernanalyse*. Master's thesis. Oslo, University of Oslo.

KARTVERKET. [c2007]. *Topografisk Norgeskart 2 WMS service*. [WMS Service]. Available from URL: <http://openwms.statkart.no/skwms1/wms.topo2?>

KLEIN, A. G. et al. 1998. Improving snow cover mapping in forests through the use of a canopy reflectance model. *Hydrological processes*. No. 12.

KOLÁŘ, J. et al. 1997. *Dálkový průzkum Země 10*. Prague, Vydavatelství ČVUT. ISBN 80-01-01567-X.

KOSKINEN, J. 2001*. Snow monitoring using microwave radars*. Helsinki, 2001. Thesis for the degrese of Doctor of Technology, Helsinky University of Technology.

KOSKINEN, J. 2010. Monitoring of Snow-Cover Properties During the Spring Melting Period in Forested Areas. *Geoscience and Remote Sensing, IEEE Transactions on*. Vol. 48, No. 1.

MAHAFZA, B. R. 2000. *Radar systems analysis and desing using Matlab.* Chapman, [c2000], 529 p. ISBN 15-848-8182-8.

MALNES, E., GUNERIUSSEN, T. 2002. Mapping of snow covered area with Radarsat in Norway. *Proceedings to IGARSS, Toronto, Canada, 24-28.june, 2002*. Available from URL: <http://projects.itek.norut.no/EnviSnow/Publications/Malnes_Earsel_2002.pdf>

MALNES, E. et al. 2004. *EnviSnow - Radar remote sensing of snow water equivalent (SWE)*. Available from URL: <http://projects.itek.norut.no/EnviSnow/D07_SWE_report_v1.0.pdf>

MARTINI, A. et al. 2006. Snow extent mapping in alpine areas using polarimetric data. *EARSeL eProceedings*.

MOEN, J., LANDMARK, B. 2008. *Satellittbasert miljøovervåkning*. Tromsø: Eureka Digital. ISBN 978-82-7389-135-8.

NAGLER, T., ROTT, H. 2000. Retrieval of wet snow by means of multitemporal SAR data. *Geoscience and Remote Sensing, IEEE Transactions on*. Vol. 38, No. 2.

NATIONAL GEOGRAPHIC et al. [2014?]*. National Geographic World Map [WMS Service]. Available from URL: <http://services.arcgisonline.com/ArcGIS/rest/services/NatGeo_World_Map/MapServer>*

NASA JPL. 1994. Radar backscatter measurements. *SIR-C Educational CD-ROM* [online]. [quoted 2014-04-10]. Available from URL:

<http://southport.jpl.nasa.gov/cdrom/sirced03/cdrom/DOCUMENT/HTML/SLIDES/MODULE02/MEASURES.HTM>

NVE. *NVE's snow pillow station* [online]. [c2007]. Available from URL: <http://www.nve.no/PageFiles/11073/prinsippskisse-av-snopute.pdf>

NVE. 2008. *Retningslinjer for hydrologiske undersøkelser: Retningslinjer for manuelle målinger av snø samt innsending av data til Norges vassdrags- og energidirektorat (NVE)* [online]. Available from URL: <http://www.nve.no/Global/Sikkerhet%20og%20tilsyn/Milj%C3%B8tilsyn/Hydrologiske%20p%C3%A5legg/15_Snomaling.pdf>

NVE. 2009. Satelittfjernmåling. *Norges vassdrags- og energidirektorat* [online]. [quoted 2013-04-25]. Available from URL: <http://www.nve.no/no/Vann-og-vassdrag/Hydrologi/Sno/Satelittfjernmaling/>

NVE. [2013?]. Senorge.no. *Senorge.no* [online]. [quoted 2013-05-04]. Available from URL: <http://www.senorge.no/>

PELLIKKA, P. K., REES, G. 2010. *Remote sensing of glaciers: techniques for topographic, spatial and thematic mapping of glaciers.* CRC Press, [c2010], xxv, 330 p. ISBN 9780203851302.

PETTINATO, S. et al. 2009. An operational algorithm for snow cover mapping in hydrological applications. *Geoscience and Remote Sensing Symposium, 2009 IEEE International, IGARSS 2009*. IEEE, 2009. IV-964-IV-967.

PIVOT, F. C. 2012. C-band SAR imagery for snow-cover monitoring at Treeline, Churchill, Manitoba, Canada. *Remote Sensing, 2012, 4*. 7: 2133-2155.

ROGNES, A. et al. 2005. Satellite based snow monitoring for hydropower production and trade in Norway – results versus operational needs. *Proceedings to ISRSE, St. Petersburg, Russia, June 2005.* Available from URL: <http://publications.nr.no/4060/Rognes_-_Satellite_based_snow_monitoring_for_hydropower_pro.pdf>

ROTT, H. et al. 2010. Cold Regions Hydrology High-resolution Observatory for Snow and Cold Land Processes. *Proceedings of the IEEE.* Vol. 98, No. 5. 752-765.

SINGH, G. et al. 2014. Capability Assessment of Fully Polarimetric ALOS--PALSAR data for Discriminating Wet Snow from Other Scattering Types in Mountainous Regions. 2014. *Geoscience and Remote Sensing, IEEE Transactions on*. Vol. 52. No. 2. 1177-1195.

ŠPÁTOVÁ, Z. 2010. *Využití dat dálkového průzkumu Země pro určování vodní hodnoty sněhu.* Master's thesis. Prague, Charles University in Prague, Faculty of Science.

STRANDEN, H.B. 2010. *Evaluering av seNorge: data versjon 1.1.* NVE. Available from URL: <http://www.nve.no/PageFiles/11067/dokument4-10.pdf>

STORVOLD, R. et al. 2006. SAR remote sensing of snow parameters in Norwegian areas - current status and future perspective. *J. of Electromagn. Waves and Appl.* Vol. 20, No. 13.

THAKUR, P. K. et al. 2013. Snow Cover Area Mapping Using Synthetic Aperture Radar in Manali Watershed of Beas River in the Northwest Himalayas. *Journal of the Indian Society of Remote Sensing.* Vol. 41 No.4. 933-945.

VALENTI, L., SMALL, D., MEIER, E. 2008. Snow cover monitoring using multi-temporal Envisat/Asar data. *Proc. 5th EARSeL LISSIG Workshop.*

APPENDIX LISTING

Appendix 1 CD